Time-Optimal Multi-Waypoint Mission Planning
in Dynamic Flow Fields

by

David Ferris

B.S. Systems Engineering, United States Naval Academy (2008)

Submitted to the Department of Mechanical Engineering
in partial fulfillment of the requirements for the degrees of

Naval Engineer

and

Master of Science in Mechanical Engineering

at the

MASSACHUSETTS INSTITUTE OF TECHNOLOGY

June 2018

© Massachusetts Institute of Technology 2018. All rights reserved.

DISTRIBUTION A. Approved for public release: distribution unlimited.

Author . . . .
Department of Mechanical Engineering
May 11, 2018

Certified by. . . . .
Pierre F.J. Lermusiaux
Professor of Mechanical Engineering and Ocean Science and Engineering
Thesis Supervisor

Accepted by . . . .
Rohan Abeyaratne
Chairman, Department Committee on Graduate Theses

Time-Optimal Multi-Waypoint Mission Planning
in Dynamic Flow Fields

by

David Ferris

Submitted to the Department of Mechanical Engineering
on May 11, 2018, in partial fulfillment of the
requirements for the degrees of
Naval Engineer
and
Master of Science in Mechanical Engineering

Abstract

This thesis demonstrates the use of exact equations to predict time-optimal mission plans for a marine vehicle that visits a number of locations in a given dynamic ocean current field. The missions demonstrated begin and end in the same location and visit a finite number of locations or waypoints in the minimal time; this problem bears close resemblance to that of the classic "traveling salesman," albeit with the added complexity of a continuously changing flow field. The paths, or "legs," between all goal waypoints are generated by numerically solving exact time-optimal path planning level-set differential equations. The equations grow a reachability front from the starting location in all directions. Whenever the front reaches a waypoint, a new reachability front is immediately started from that location. This process continues until one set of reachability fronts has reached all goal waypoints and has returned to the original location. The time-optimal path for the entire mission is then obtained by trajectory backtracking, going through the optimal set of reachability fields in reverse order. Due to the spatial and temporal dynamics, a varying start time results in different paths and durations for each leg and requires all permutations of travel to be calculated. Even though the method is very efficient and the optimal path can be computed serially in real-time for common naval operations, for additional computational speed, a high-performance computing cluster was used to solve the level set calculations in parallel. This method is first applied to several hypothetical missions. The method and distributed computational solver are then validated for naval applications using an operational multi-resolution ocean modeling system of real-world current fields for the complex Philippines Archipelago region. Because the method calculates the global optimum, it serves two purposes. It can be used in its present form to plan multi-waypoint missions offline in conjunction with a predictive ocean current modeling system, or it can be used as a litmus test for approximate future solutions to the traveling salesman problem in dynamic flow fields.

Thesis Supervisor: Pierre F.J. Lermusiaux
Title: Professor of Mechanical Engineering and Ocean Science and Engineering

Acknowledgments

My completion of this thesis is only possibly through the support of family, friends, and colleagues. I'll do my best to thank them all.

First, I'd like to thank my mother, Cheryl, who has always encouraged me to do my best, no matter the difficulties. My father, Ron, passed away during my time here at MIT, and continues to be missed. As my father, coach, and boss, he helped me become the man I am today. For that I'll always be grateful.

I'd like to thank the United States Navy for providing me this opportunity at MIT. My 2N classmates have made these three years a wonderful tour of duty, full of laughs to make the struggle a little easier.

My wife, Lisa, and daughters, Nina and Eva, are the joys of my life. I couldn't imagine completing my time at MIT without them.

Mike Benjamin and his autonomy course (2.680 Unmanned Marine Vehicle Autonomy, Sensing, and Communication) were a huge inspiration for this work. Though my focus shifted away from general autonomy and working in MOOS-IvP, I still think of his class as a defining part of my MIT experience. Had there been more time, I would have liked to incorporate my mission planning results into a real-world mission using the MOOS-IvP platform.

Dr. Pierre Lermusiaux, who leads the Multidisciplinary Simulation, Estimation, and Assimilation Systems (MSEAS) group was a great advisor to work with. He understood my limits and goals, and he gave support whenever needed. His early inputs saved a lot of time and effort by starting me on a great path early on.

Dr. Deepak Subramani's continued support allowed my thesis to happen. He was always open to discuss everything from big picture theory and ideas to the small details of Matlab code, parallel processing on the cluster, thesis structure, and Latex intricacies.

Patrick Haley, Chris Mirabito, Chinmay Kulkarni, and Corbin Foucart all deserve a special thanks for their help learning the intricacies of the underlying Matlab code, the MSEAS cluster, as well as numerous details spread throughout this thesis.

Finally, praise be to God for all the blessings in my life.

Contents

List of Figures

List of Tables

Chapter 1

Introduction

1.1 Motivation

Autonomous underwater vehicles (AUVs) are currently fielded world-wide by commercial companies, militaries, and research institutions, and their use will only increase in the coming years. Publicly, the United States Navy has released its Unmanned Underwater Vehicle (UUV) Master Plan and it's Autonomous Undersea Vehicle Requirements for 2025 [US Navy, 2004; US Navy Undersea Warfare Directorate, 2016]. These documents lay out the acquisition strategy for the family of underwater vehicles the future Navy needs. Figure 1-1 is a visual representation of the Navy's UUV acquisition plan as of April 2018. The Navy is committed to acquiring and deploying these vehicles as quickly as possible, while improving their on-board autonomy through research and development.

There have also been recent organizational shifts which emphasize unmanned systems within the Navy. On Sept. 26, 2017, the US Navy stood up Unmanned Undersea Vehicle Squadron 1, or UUVRON1, which is the first squadron dedicated to UUVs [Ziezulewicz, 2017]. On Mar. 22, 2018 the Navy renamed Program Executive Office Littoral Combat Ship (PEO LCS) to PEO Unmanned and Small Combatants, better reflecting the full breadth of that office's oversight of unmanned surface and subsurface systems

In short, the "unmanned" are coming - the hardware and vehicles are on the way. The motivating question is, "How can we deploy these present and future vehicles more intelligently through mission planning to better achieve mission success?" While mission planning is important for both surface and sub-surface vehicles, this thesis will focus on the undersea environment where communication is limited and a vehicle can receive mission updates on a much slower time-scale.

In 2009, the US Navy sponsored a RAND corporation survey of UUV missions
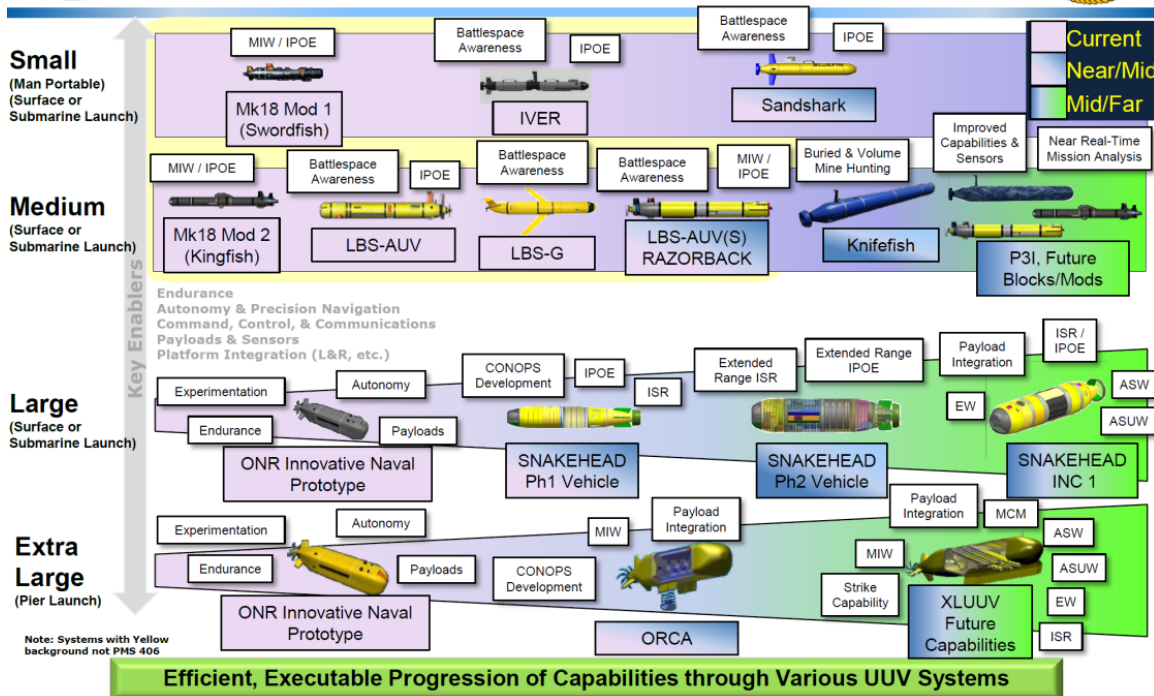
Figure 1-1: The US Navy has aligned all UUV acquisition efforts so that many independant program offices are not duplicating efforts, and that investments in research and technology are shared across platforms.

[Button et al., 2009]. Below are the seven mission areas recommended in the report:

1. Mine countermeasures (MCM)
2. Leave-behind surveillance sensors or sensor arrays
3. Near-land and harbor-monitoring
4. Oceanography
5. Monitoring undersea infrastructure
6. Anti-submarine warfare (ASW) tracking
7. Inspection/identification

Considering only gross navigational requirements, mission areas 2, 3, and 5 involve a vehicle traveling to specific locations in the ocean, or "multi-waypoint missions." Mission areas 1 and 6 can be characterized as "reactionary missions," requiring a UUV to adapt to the situation based on sensor inputs, while areas 4 and 7 could be a considered a hybrid of the two extremes.

The focus of this thesis will be to support those multi-waypoint missions by ensuring UUVs take the optimal path in a realistic current environment. Path planning

in ocean currents is especially important for UUVs due to their operating speeds relative to current speeds. Ocean currents of 1-2 knots are common, and currents can be higher in littoral areas [Lermusiaux et al., 2011]. Propelled UUVs typically operate between 2-5 knots and the majority of their power supply is dedicated to propulsion. Slower vehicles, such as buoyancy gliders and wave gliders, have longer durations, but may not be able to overcome even small currents. [Liao et al., 2016; Chien-Chou et al., 2014]. Complicating mission planning further, ocean currents are dynamic, changing speed and direction within the time frame of typical UUV missions. Therefore, a UUV mission planner optimizing for time or energy must take these currents into account.

Recent work has developed partial differential equations (PDEs), efficient numerical schemes and computational systems to compute exact time-optimal paths in certain ocean currents [Lolla et al., 2012, 2014a,b; Lermusiaux et al., 2016]. These methods have been used to demonstrate path planning in realistic ocean re-analysis, and in real-time with real UUVs [Subramani et al., 2017b; Lermusiaux et al., 2017a,b]. This method can improve a vehicle's point-to-point travel time, but no method has been demonstrated which applies this time-optimal path planning to overall mission planning for multi-waypoint missions.

1.2   Overview

Chapter two describes an introductory background to UUV autonomy and mission planning. Chapter three describes how this specific problem has been framed. It also details the intended use case for this thesis. Chapter four describes the method used to integrate past work in Time-Optimal Path Planning with a Traveling Salesman Problem framework. Chapter five demonstrates the experimental results of several test cases as well as several missions planned using a model of real-world current data representing the Philippines Archipelago region. Chapters six concludes this thesis and proposes several areas in which this work could be expanded in the future.

Chapter 2

Background

2.1 Autonomy

Marine vehicle autonomy has been a field of rapid research and growth in recent years. While there are numerous areas of autonomy, the dominant component of marine autonomy is navigation. Navigation autonomy can range from simple compass heading control to complex autonomy balancing desires of collision avoidance, mission requirements, fault-tolerance, sensor fusion and efficiency [Gerlack, 2015; Woerner, 2017; Leavitt, 2017]. There is a great deal of research in all of these areas. However, no amount of on-board intelligence will guarantee an optimal mission plan for a marine vehicle without considering the surrounding ocean environment.

2.2 UUV Mission Planning

The most basic UUV mission planning software takes location inputs from the user and transforms those inputs into propulsion and heading control signals. Ignoring currents, this will result in a planned distance and duration for the mission. Prior to launch, the human planner or the planning software must estimate the vehicle's energy usage along that path and ensure there is an adequate margin of safety for the vehicle to be recovered before power is exhausted.

In basic systems, energy usage can be estimated using the cube law characteristic of velocity and speed. The "hotel" loads which power control systems, and sensors can be assumed constant over the mission. In more advanced systems, a UUV can have a complex internal model of its own propulsion system's energy usage as well as the hotel load variation through a mission profile [Carolis et al., 2014; Carolis, 2017].

2.3　Optimal Mission Planning

There is no true "completely-optimal" path for a vehicle to take in a real-world dynamic environment because there are so many trade-offs for a mission planner. Many of these trade-offs rely on a user's opinion an not objective, measurable quantities. There are trade-offs between speed, energy, safety, mission effectiveness, risk, cost, etc. For example, would you want your vehicle to take a path which has a high likelihood of success but low likelihood of recovery or a medium likelihood of success with high likelihood of recovery? Should the vehicle take the fastest path or the path most likely to avoid detection? Should the vehicle complete its mission as quickly as possible or maximize its energy reserve so that its tasking can be updated throughout the mission?

In order to build the tools which present these choices to a future operator or autonomy software, some base capability must be created. This thesis intends to support creation of that capability by showing the time-optimal path for a multi-waypoint mission. For clarity with respect to this thesis - the words "path planning" will be used to describe the travel between a starting point (A) and ending point (B). "Mission planning" will be used to describe the travel between a number of paths from the start of a mission (A), through many waypoints (B, C, D, etc.), to the completion of a mission (back to A). Three ways to determine those paths between points could be Time-Optimal Path Planning, Energy Optimal Path Planning, and Path Planning with Uncertainty.

2.3.1　Time-Optimal Path Planning

Of the three methods discussed here, Single Speed Time-Optimal Path Planning (TOPP) is the most straightforward and requires the lowest amount of computation time per path. A demonstrated TOPP methodology is to use level set equations to grow a "reachability front" from the starting location, expanding the front at each time interval, until all desired goal locations have been reached. This reachability front represents the furthest points a vehicle could reach at any given time, as shown in Figure 2-1. Whenever the reachability front has reached a given target, that is the earliest point in time possible for that target to be reached along any path. A particle tracking equation is then solved backward from that time to produce the required headings at all times along the time-optimal path. This process has been shown to provide good results and is the foundation of the current work of this thesis [Lolla et al., 2014a,b, 2015].

It is important to emphasize that this method can be useful even in the absence
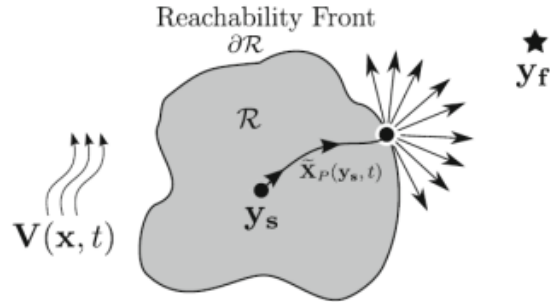
Figure 2-1: The reachability front can be represented by a level set equation which grows from the origin until it reaches all objectives [Lolla et al., 2014b].

of currents. Geographically complex areas with many areas a vehicle needs to avoid can present an operator or autonomy software with the difficult task of navigating through the many possible routes. Figure 2-2 shows an example of many gliders navigating through a complex island chain [Lolla et al., 2014a,b].

2.3.2 Energy-Optimal Path Planning

While time is important, it is more likely that energy is the limiting factor for a given UUV mission. If the operator were to allow a range of speeds throughout a path, there are an infinite number of paths which could feasibly reach the target at a given time. Energy-Optimal Path Planning (EOPP) extends the TOPP method above to a stochastic PDE-based optimization to compute minimum energy paths among time-optimum paths [Subramani and Lermusiaux, 2016; Subramani et al., 2017a].

2.3.3 Path Planning with Uncertainty

In reality, all current prediction models will have inherent uncertainty, and these path planning methods have so far assumed the current model is correct. Therefore, a chosen path may be better or worse than the real-world optimum. In order to incorporate this risk, a method has been demonstrated which grows a reachability front represented by not just one level set equation, but rather represented by stochastic level-set partial differential equations [Subramani et al., 2018]. This method outputs a range of possible paths for a range of risk tolerance from high-risk/high-reward paths to low-risk/low-reward paths and everything in between.
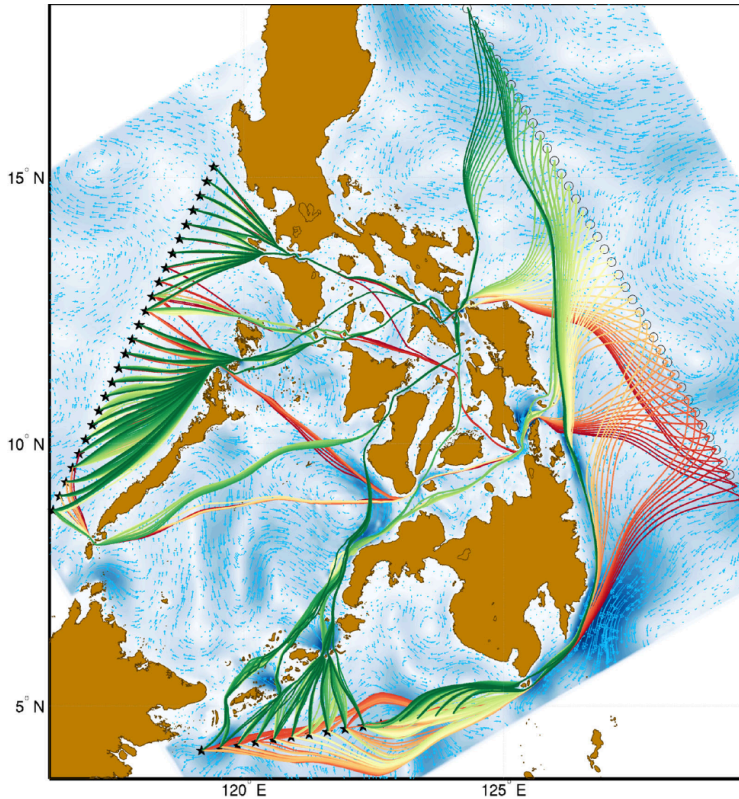
Figure 2-2: Multiple paths through a complex island chain. These paths would still be difficult to plan regardless of current [Lolla et al., 2014a].

2.4   Traveling Salesman Problem

The traveling salesman problem has been of interest to mathematicians and researchers for decades. Solutions to growing problem sizes were published regularly over the years from a 49-city problem in 1954 up to that of 24,978 cities in 2004. There are numerous books, papers, and theses related to the problem [Lam, 2005; Applegate, 2006]. For large numbers of cities it becomes computationally infeasible to assess all permutations of travel through brute force methods.

The power supply of a realistic UUV is limited, and therefore a mission with dozens, hundred, or thousands of waypoints would require those waypoints to be close together. As the distance between points decreases, the time-optimal path in a dynamic current tends toward a straight line path. Therefore for realistic vehicles and currents, the standard TSP solutions would be appropriate when large numbers of cities are used. Additionally, due to the computational growth discussed in Chapter 4, the focus of this study is not solving many-city TSP, but to constrain the problem to lower numbers where all permutations of travel may be accessed in a brute force but efficient and exact method.

2.5   Local versus Global Optimum

Even within the framework of using reachability front calculations for each leg, there are several assumptions and methods which could be employed to reduce the computational requirements of this problem while leading to local optimum solutions. For example, a four-waypoint mission solution space would contain 24 possible tours as seen in Table 2.1. Of those, 6 tours would travel from B to C (underlined), and 6 from C to B (bold). If you assume that the calculation can only be "shared" when the starting time is the same, then 10 calculations are needed for all options of B-C and C-D start times. If, however, you assume that the B-C travel time is constant or that even the B-C and C-B travels times are equal, the computation time is lowered. This, however, does not guarantee a global optimum solution. It is the goal of this thesis to determine global optimum solutions rather than improve computational speed through assumptions. Future work may investigate the trade-offs between these goals.

A<u>BC</u>DEA	A**CB**DEA	ADB<u>CE</u>A	AEB<u>CD</u>A
A<u>BC</u>EDA	A**CB**EDA	ADBECA	AEBDCA
ABDCEA	ACDBEA	AD**CB**EA	AE**CB**DA
ABDECA	ACDEBA	ADCEBA	AECDBA
ABECDA	ACEBDA	ADEB<u>CA</u>	AEDB<u>CA</u>
ABEDCA	ACEDBA	ADE**CB**A	AED**CB**A

Table 2.1: All 24 permutations of a mission which starts at point A, travels to four waypoints (B, C, D, & E), and returns to point A. Legs which travel from BC are underlined and CB are in bold. If these leg durations were assumed to be constant, the problem would simplify, but the solution would no longer be guaranteed to be the global optimum.

2.6   Philippines Archipelago Current Model

All of the path planning methods described in 2.3.1 through 2.3.3 require an a priori current model of the operating area. The most useful operating areas would be large enough in scale to demonstrate future Large Diameter (LDUUV) and Extra Large Diameter (XLUUV) Unmanned Underwater Vehicles. To highlight the benefits of this mission planner, the area would contain interesting geography and currents. One such current model was selected from earlier research modeling ocean dynamics in the Philippine Archipelago region [Burton, 2009; Lermusiaux et al., 2011]. Figure 2-3 shows the boundary of the current model overlaid on the actual Philippines geography.

The red points indicate locations of real world US Navy Shipwreck sites, as found in open source websites. These locations will be used in Chapter 5 to demonstrate UUV missions in realistic currents.
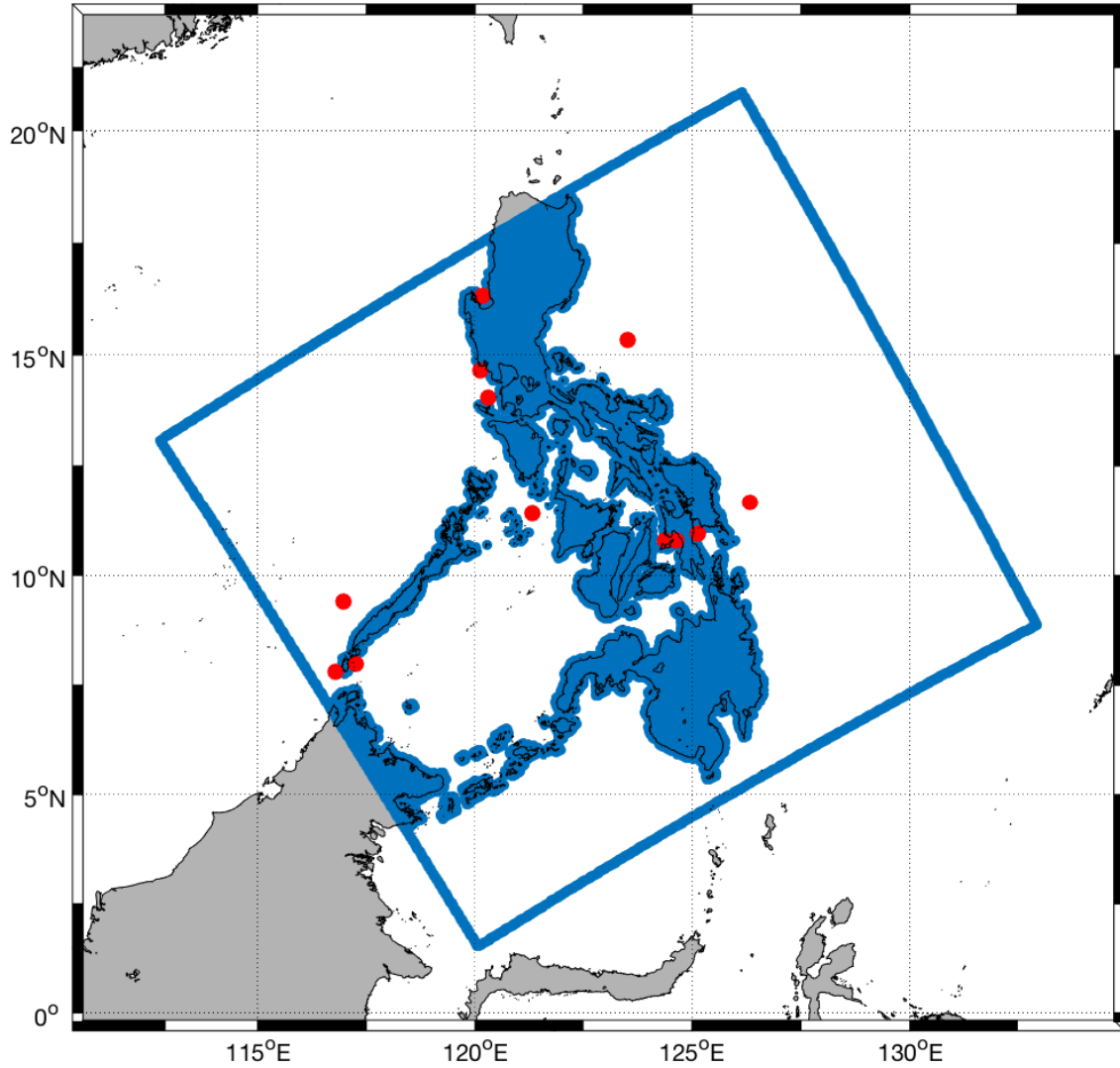
Figure 2-3: The current data set used in this work was derived from earlier research modeling the Philippines Archipelago [Lermusiaux et al., 2011]. The data is bounded by the outer box as well as the land "mask" shown in blue. The red points indicate locations of real-world US Navy shipwreck locations.

Chapter 3

Problem Statement

3.1 Mission Definition

It is important to clearly define what is meant by a mission when discussing how to optimize mission performance. The following mission types were developed for consideration. Ultimately, the first mission type shown below was chosen as the most relevant for this topic.

3.1.1 Unlimited Missions

The following mission types could be explored with no limit in mind regarding time or energy. It would be relatively straightforward to adjust the current method from a standard TSP problem to investigating types 2 and 3.

1. The vehicle begins and ends at the same location.

2. The vehicle begins at a "drop off" location and ends at a "pickup" location.

3. The vehicle is not recovered. The mission begins in one location and ends when all targets are visited.

3.1.2 Time and Energy Limited Missions

All of the above mission types could also be explored with the additional constraints of maximum time and/or energy usage. This would require additional front growth calculations after reaching every waypoint to ensure the vehicle can return to it's pickup location without exceeding its limit. The problem with implementing this limit is not conceptual but computational. The number of front growth calculations in this case, $J_{lim,n} = J_n + n + n * J_{lim,n-1}$, where $J_{lim,n=0} = 1$. A comparison of mission

Number of Waypoints	Number of Tours	Unlimited Mission Front Computations	Time-Limited Mission Front Computations
n	$n!$	$J_n = 1 + n * J_{n-1}$	$J_{lim,n} = J_n + n + (n * J_{lim,n-1})$
1	1	2	2
2	2	5	7
3	6	16	25
4	24	65	105
5	120	326	531
6	720	1957	3193
7	5040	13700	22359

Table 3.1: In order to incorporate a time limit for a give mission, the mission planner would need to calculate if the vehicle can return to the starting point after each leg of a tour. Thus a time-limited mission would increase the number of computations required, but only by a factor of less than 2.

types can be seen in Table 3.1. This corresponds to work done on the Orienteering Problem and could be an area of future study [Gunawan et al., 2016].

3.2 Related Missions

There are numerous other related missions to which the travelings salesman concept could be applied in dynamic currents. For example, a swarm of vehicles could travel together while maintaining a required formation [Lolla et al., 2015]. Instead of stationary targets, there could be moving targets for ship interception missions and/or moving obstacles to avoid [Mirabito et al., 2017; Lolla et al., 2015]. Risk can be incorporated into the path planning to account for uncertainties in the current model [Subramani and Lermusiaux, 2018]. Finally, data learned from the vehicle's onboard power supply can be used to improve mission performance [Edwards et al., 2017]. Advanced autonomy software of the future may rely on certain aspects of all of these foundational mission types.

3.3 Deployment Construct

It is generally accepted that most UUVs can be launched from a surface vessel and have a mission duration measured in hours to days. The Navy expects to deploy a prototype of its ship and submarine-launched LDUUV in 2019 with an expected duration of five days. The concept for the US Navy's XLUUV will be a large, pier-

launched vessel with mission durations measured in weeks, up to 30 days. Therefore missions will be limited to 5 days when starting in open water and 30 days when starting from land. A vehicle speed of 3 knots (1.54 m/s) will be assumed for all missions.

3.4   Software Requirements

It is assumed that a predictive current model of the operating area has already been developed prior to application of these methods. The predictive current model will be most effective with up to date and accurate measurements of the current condition. Therefore, the model would be developed as close as possible to the vehicle's deployment time. At this point, the mission planning method outlined in this thesis would be used to determine the time-optimum path the vehicle will travel. That path would then be loaded into the vehicle's navigation software prior to launch.

For this thesis, we employed the MSEAS software (http://mseas.mit.edu/software). MSEAS [Haley and Lermusiaux, 2010; Haley et al., 2015] is used for fundamental research and for realistic simulations and predictions in varied regions of the world's ocean [Leslie et al., 2008; Onken et al., 2003; Haley et al., 2009; Ramp et al., 2009; Lermusiaux et al., 2011, 2017a,b]. Applications include monitoring [Lermusiaux et al., 2007], real-time acoustic predictions and data assimilation [Xu et al., 2008; Lam et al., 2009; Duda et al., 2011], and ecosystem predictions and environmental management [Beşiktepe et al., 2003; Cossarini et al., 2009]. Examples of real-time sea experiments include: AWACS and SW-06 [Haley and Lermusiaux, 2010; Colin et al., 2013]; AOSN-II and MB-06 [Lermusiaux et al., 2006; Gangopadhyay et al., 2011; Ramp et al., 2011]; QPE-08 and -09 [Lermusiaux et al., 2010; Gawarkiewicz et al., 2011; Lermusiaux et al., 2018]; PhilEx-08 and -09 [Agarwal and Lermusiaux, 2011; Lermusiaux et al., 2011](e.g. Agarwal and Lermusiaux, 2011; Lermusiaux et al., 2011); and NASCar and FLEAT [Lermusiaux et al., 2017a; Pan and Lermusiaux, 2018].

At the core of MSEAS are three solvers of governing fluid and ocean dynamics equations. The first solver is part of an extensive modeling system for hydrostatic primitive-equation dynamics with a nonlinear free surface, based on second-order structured finite volumes [Haley and Lermusiaux, 2010]. It is used to study and quantify tidal-to-mesoscale processes over regional domains with complex geometries and varied interactions. The MSEAS capabilities include: fast-marching coastal objective analysis [Agarwal and Lermusiaux, 2011]; estimation of spatial and temporal scales from data [Agarwal, 2009]; initializations of fields and ensembles [Lermusiaux et al., 2000; Lermusiaux, 2002; Haley et al., 2015]; nested data-assimilative tidal prediction

and inversion [Logutov and Lermusiaux, 2008]; implicit two-way nesting and tiling [Haley and Lermusiaux, 2010]; stochastic subgrid-scale forcing [Lermusiaux, 2006]; adaptive data assimilation, sampling and learning [Lermusiaux, 2007; Schofield et al., 2010]; biogeochemical modeling [Beşiktepe et al., 2003]; Lagrangian coherent structures and their uncertainties [Lermusiaux et al., 2006]; many-task computing [Evangelinos et al., 2011]; and systems for the control of such legacy codes [Evangelinos et al., 2006]. Integral to our uncertainty prediction is our Error Subspace Statistical Estimation for ensemble forecasting and data assimilation [Lermusiaux, 2006, 2007]. We also compare predictions to data: examples include physical-biogeochemical forecasts for the Philippines Archipelago [Lermusiaux et al., 2011]; uncertainty forecasts for the Taiwan region during the Quantifying, Predicting and Exploiting (QPE) uncertainty DRI [Gawarkiewicz et al., 2011; Lermusiaux et al., 2010, 2018]; and stochastic reachability, path planning and adaptive sampling forecasts for gliders and floats during NASCar [Lermusiaux et al., 2017a]. Recently, we also implemented the DO primitive-equations for stochastic ocean predictions [Subramani, 2018; Subramani and Lermusiaux, 2018].

The other two MSEAS solvers are non-hydrostatic fluid and ocean dynamics models. One is a simple 2D model using conservative finite-volumes implemented in Matlab Ueckermann and Lermusiaux, 2012. This simple 2D model has been very useful for diverse ocean-dynamics process studies and for the incubation of advanced schemes and methodologies. The other model is a non-hydrostatic 3D Navier-Stokes and Boussinesq code using the finite-element method. Specifically, novel Hybridizable Discontinuous Galerkin finite-element schemes were combined with projection methods for Navier-Stokes and Boussinesq non-hydrostatic primitive-equations [Ueckermann, 2014; Ueckermann and Lermusiaux, 2016; Ueckermann et al., 2018]. These models can be employed for targeted non-hydrostatic biogeochemical process-studies, focusing on the variability of sub-mesoscale pathways and mixed-layer processes.

Chapter 4

Theory and Schemes

The major effort of this thesis was the integration of a Time-Optimal Path Planning (TOPP) methodology with a Traveling Salesman Problem (TSP) framework. Once that integration was complete and results were obtained, the focus shifted to improving efficiency by computing reachability front calculations in parallel on a cluster.

4.1   TOPP Integration with TSP

The TOPP method used was originally created to determine the time-optimal path between two points, given a known starting time and current model. It has not, however, been applied to a traveling salesman problem until this point. In this traveling salesman construct, if n is the number of waypoints to visit, the number of possible tours grows as $n!$ and the number of legs within each tour is equal to $n+1$. Therefore the goal of the mission planner is to fill an $n!$ by $(n+1)$ matrix with the individual leg times, and determine the minimum total time of all possible tours. Due to that fact that a single reachability front calculation can start from one origin and determine the time-optimal path to n waypoints, there are less than $n!*(n+1)$ front calculations required. The number of front calculations or "jobs", $J_n = 1 + n*J_{n-1}$, where $J_0 = 1$, as seen in Table 4.1.

For a given mission, a list is created showing all permutations possible through all waypoints. Once all permutations are known, the mission planner works from beginning to end along all tours, calculating the duration of each leg of the tour as required. As discussed in 2.5, each reachability front job can be calculated once it's starting time is determined by the previous job.

Way-points	Tours	Reachability Front Calculations, $J_n =$	Series Computation Time [hrs], $T_{series} =$	∞-Core Computation Time [hrs], $T_\infty =$	100-Core Computation Time [hrs], $T_{100} =$
n	$n!$	$1 + n * J_{n-1}$	$T_{ave} * J_n$	$T_{ave} * (n+1)$	$approximated$
1	1	2	1	1	1
2	2	5	2.5	1.5	1.5
3	6	16	8	2	2
4	24	65	32.5	2.5	2.5
5	120	326	163	3	4
6	720	1957	978.5	3.5	12.5
7	5040	13700	6850	4	71.5

Table 4.1: The standard computational explosion of the Traveling Salesman Problem is further accelerated by the requirement to compute a reachability front for determining all leg durations. The total computation times shown assume an individual computation time, $T_{ave} = .5$ hours

4.2 Parallel Computing of Reachability Fronts

A single laptop can process an entire mission in series, but the vast majority of computations can be done in parallel. The only requirement to start a job is that its immediately preceding job is complete. Therefore, the maximum number of jobs which can be ran in parallel is equal to the number of tours, $n!$. The benefits of parallel processing increase with the current model's grid size as well as the number of waypoints. Figure 4-1 shows that 16 jobs are required for a 3-waypoint mission. All horizontal rows of jobs can be accomplished in parallel, and the vertical paths from beginning to end show all possible tours for the mission.

While the number of parallel jobs can be equal to the number of tours, there is also a practical limit of how many jobs a given computing cluster may process in parallel. Beyond a hard-coded limit assigned to a user by the cluster's administrator, there are practical limits due to the fact that the solver is constantly referencing data saved to file locations on a hard drive. The "needle" can only move so fast and the I/O throughput becomes the true bottleneck to the computation. As will be shown in Chapter 5, good results were obtained for up to six-waypoint missions processing 720 tours in parallel without manually controlling the amount of jobs submitted. However the cluster's scheduling software, Sun Grid Engine, maintains the number of jobs actually executing below the number of open cores available. Improvements to this aspect of the parallel processing software were not addressed in this research.
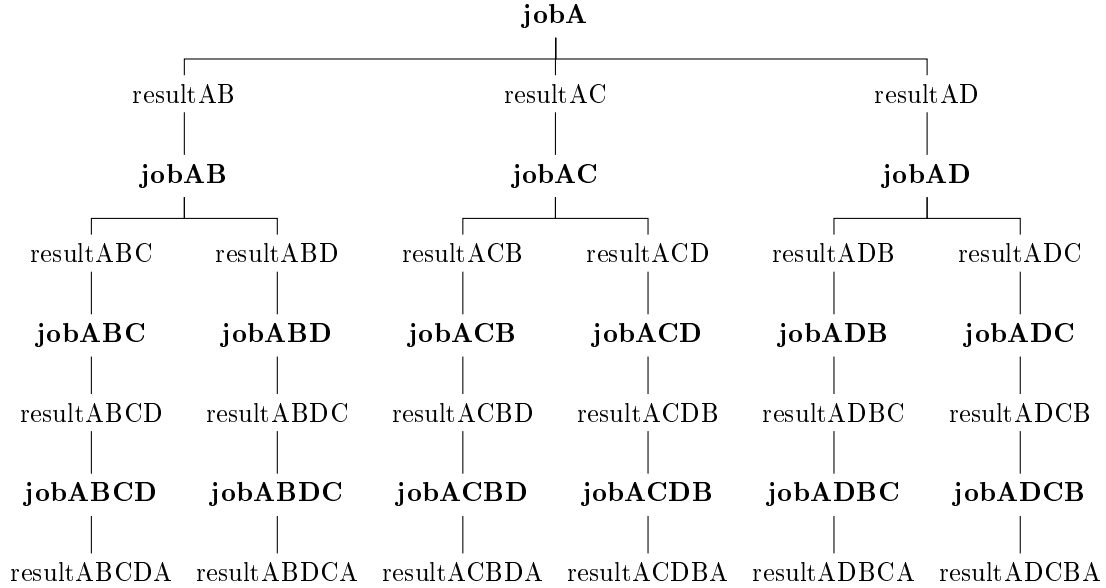
Figure 4-1: To improve total mission computation speeds, reachability front calculations are broken down into as many parallel jobs as possible. Any job can start as soon as the results of its preceding job have been saved. This figure demonstrates the job flow for a three-waypoint mission.

4.3 Foundational Code

To simulate real-world UUV missions, a current model was used which represents the currents and geography of the the Philippines Archipelago. This current model consists of a grid 1518 km x 1671 km with velocities captured every 3 km and every 3 hours. This data was generated from a higher fidelity, multi-resolution model developed in previous research [Burton, 2009; Lermusiaux et al., 2011].

The "current model" exists as a folder of .mat files containing u and v velocities for each point in a grid. The goal of the main solver function is to grow a level set equation from the starting point until all goal locations are reached. The level set represents the reachability front for the vehicle so that at any point in time the vehicle can reach any location within the level set. In order to grow the level set equation, the vehicle's speed is combined with the current speed at each location along the level set. To resolve a solution with finer temporal resolution than the original .mat files represent, the current velocities are interpolated between the previous and next u and v values for every point in the grid. To solve at a finer spatial resolution, the current velocities are advected using a C++ advection code.

In order to create a mission planner, the original TOPP code was modified to more flexibly accept varying start locations, start times, and goal destinations, as well as to save the solver outputs into specified filenames for use later. This allowed

a unique "job," or reachability front calculation, to be created with whatever starting conditions the mission planner requires. A job is submitted to the compute cluster's scheduler, Sun Grid Engine (SGE), whenever its predecessor job's results have been saved. Each SGE job is very simple, and consists only of the following four commands:

1. Open Matlab
2. Set $history = XYZ$,
   where "XYZ" is replaced by the job's history within the mission
3. Run a Matlab script, "job_template.m"
4. Exit Matlab

The actual reachability front calculation is performed within this job_template.m Matlab script and the results are saved in the appropriate format in order for the cluster oversight script to know when to commence the following jobs. The general process of job_template.m consists of the following:

1. Initialize variables and run setup scripts
2. Load pre-generated tour permutation list
3. Use "history" input to determine where job lies with the overall mission
4. Set locations for the start of front growth and goal waypoint(s)
5. Load mission start time from results file of a previous front growth
6. Run TOPP algorithm
7. Save results for times, paths, currents, headings in appropriate filenames
   (i.e. resultABC, flowsABC, etc.)

4.4   Gathering Results

Once all result files have been generated, the n! by (n+1) matrix of leg times is complete. The minimum total time for a given tour is selected as the optimum tour. The corresponding optimal path can then be saved, plotted, or used as waypoint inputs to a UUV navigation software. For viewing results, all heading, flow, and path data has been saved for all jobs, and thus, all possible paths can be recreated. Chapter 5 shows several examples of these outputs.
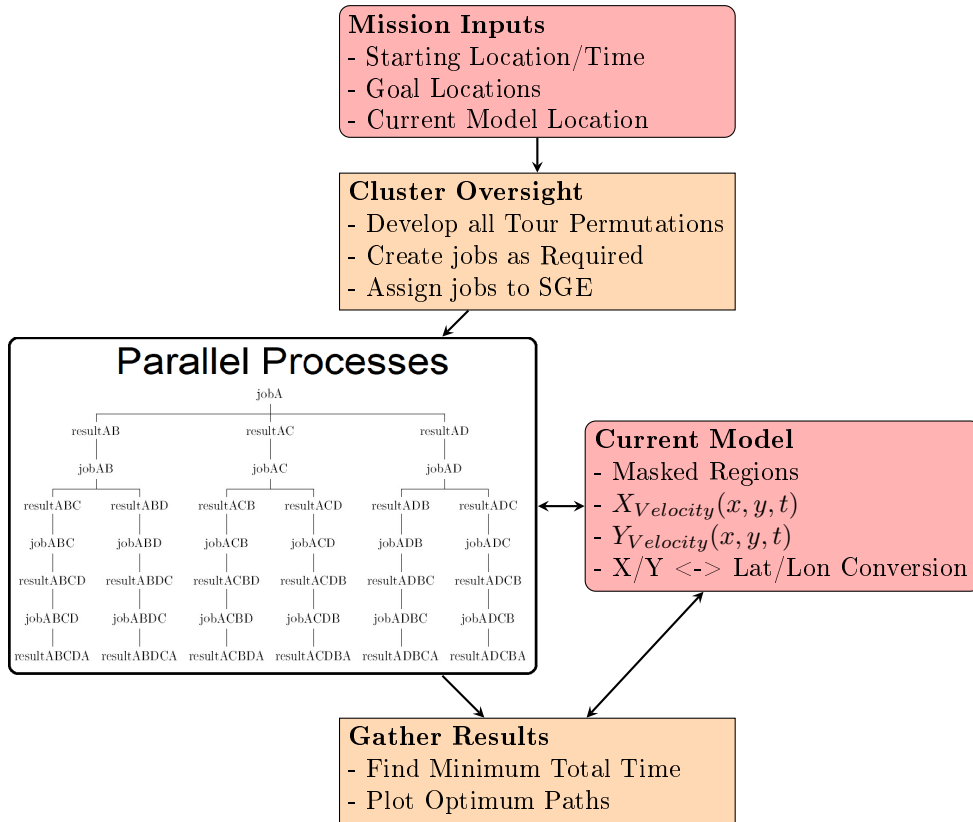
Figure 4-2: The calculations for an entire mission are started by one script which takes user input for a mission's starting configuration. The user inputs are used to begin a cluster oversight script which generates individual reachability front calculations to be completed by the computing cluster in parallel. All jobs reference the same data within the current model to complete their calculations.

Chapter 5

Applications

Three hypothetical test cases are presented below to help illustrate the method. These are followed by several example missions with realistic conditions located in the Philippines Archipelago operating area.

5.1 Test Cases

The three test cases below highlight different aspects of the method. Test Case 1 shows how various constant currents will affect mission outcomes of a very basic two-waypoint mission. Test Case 2 shows how time-varying currents play a role in a three-waypoint mission. Test Case 3 gives a visualization of how the parallel growth of reachability fronts are occurring. These test cases are all non-dimensional and are used to build intuition and gain insights.

5.1.1 Test Case 1: River Crossing Example

The following three examples show how currents play a role in a hypothetical river crossing mission. The vehicle must cross the river, reach two waypoints, and return back. Initially, the river has no current, and it makes no difference which order the waypoints are visited, as shown in Figure 5-1. Next, a constant East current is applied with magnitude, $U_{current} = .5*V$, where V is the vehicle velocity. V is assigned in the Mission Setup script and is assigned a non-dimensional value of 1. In this case, there is a slight benefit to traveling in the clockwise path. Finally, a "river-like" current is applied with magnitudes along the center, $U_{center} = .75*V$ and edge, $U_{edge} = .25*V$. In this case, the vehicle improves the total time by 20% by choosing the ACBA route. The current distorts the reachability fronts as they grow. Therefore the time-optimal paths follow the lowest velocity along the Northern shore and are not straight paths.
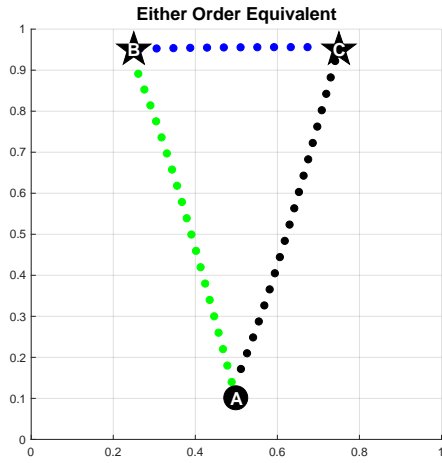
(a) Zero current

	Path	ABCA	ACBA
Zero Current	Total Time*	**1.64**	**1.64**
	% of Optimum**	100%	100%
Constant Current	Total Time*	**2.01**	2.05
	% of Optimum**	100%	102%
"River-like" Current	Total Time*	2.17	**1.81**
	% of Optimum**	120%	100%

* All times are unitless.
** Obtained by dividing tour duration by minimum duration for given scenario.

(b) Comparison of Times
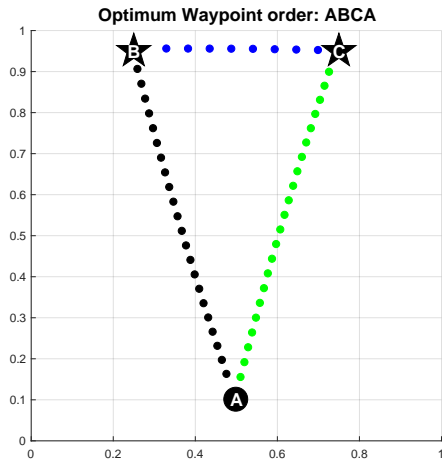
(c) Constant current toward right
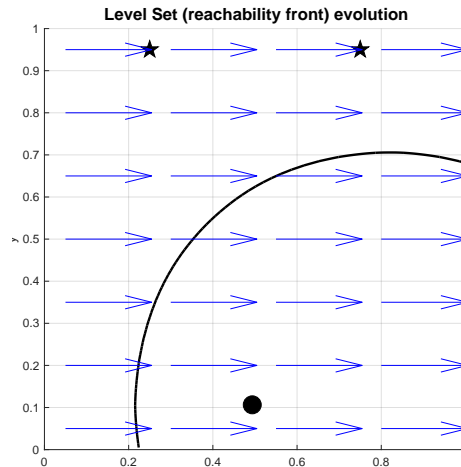
(d) Constant current front evolution
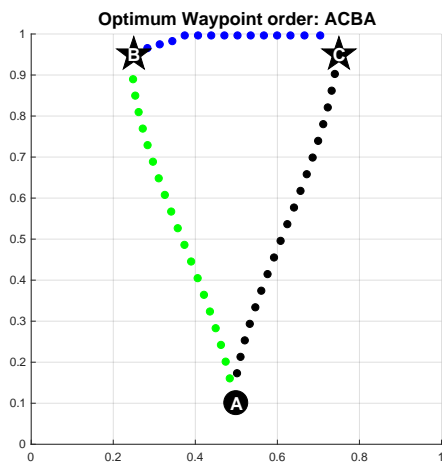
(e) River-like current
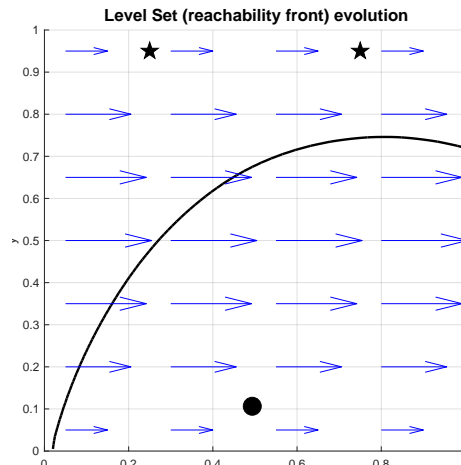
(f) River current front evolution

Figure 5-1: Three Examples of a River Crossing Scenario

5.1.2   Test Case 2: Time-Varying Current Example

While the previous example demonstrated how a current's spatial dynamics affect mission outcomes, the next example will demonstrate how temporal dynamics affect the outcomes. In this example, the vehicle starts from a central location and visits three surrounding waypoints. The vehicle starts at $(0, 0)$, and the goal waypoints are spaced at $(.25, .25)$ intervals on a dimensionless grid from 0 to 1. The current has a non-dimensional magnitude of approximately $U_{current} = .5 * V$, where the vehicle velocity is again, $V = 1$. The current direction varies sinusoidally between Southwest and Northwest, as shown in Figure 5-2. The resulting times and optimal paths are shown in Figure 5-3. Initially, when no current exists, the paths of ABCDA and ADCBA are equivalent. When a current is introduced with a time period, $T_{current} = 1$ (approximately the total mission time), these paths differ, and ABCDA takes 19% longer to complete than the optimum, ADCBA. Of note, this new optimum takes less time to complete than any of the original paths with no current. Finally, the frequency of the current is increased by 50% of the original frequency. In this environment, the optimum path becomes ADBCA which goes against intuition and the previous results. If an operator chose an intuitive, shortest distance path, the mission would take over 11% longer to complete, even when taking time-optimal paths for each leg.

(a) Snapshot 1   (b) Snapshot 2   (c) Snapshot 3   (d) Snapshot 4   (e) Snapshot 5
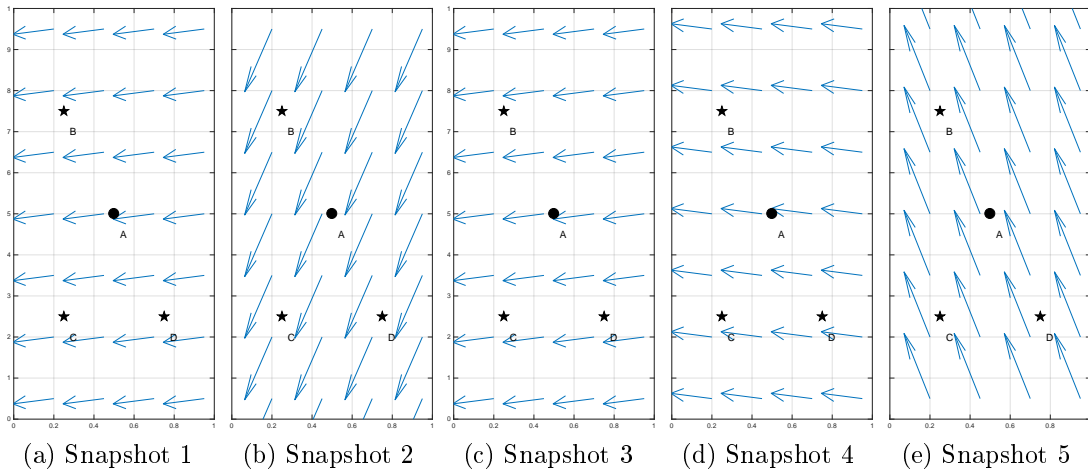
Figure 5-2: These snapshots show a current which varies sinusoidally through time between Southwest and Northwest. For this test case, the frequency which the currents shifts was varied, but the magnitudes were not changed.
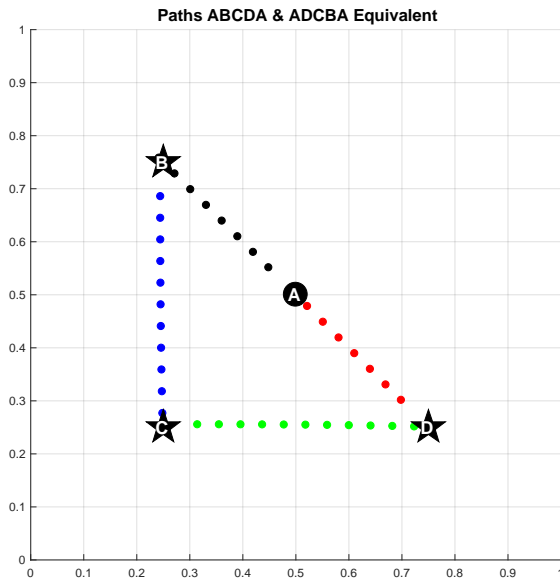
(a) Zero Current
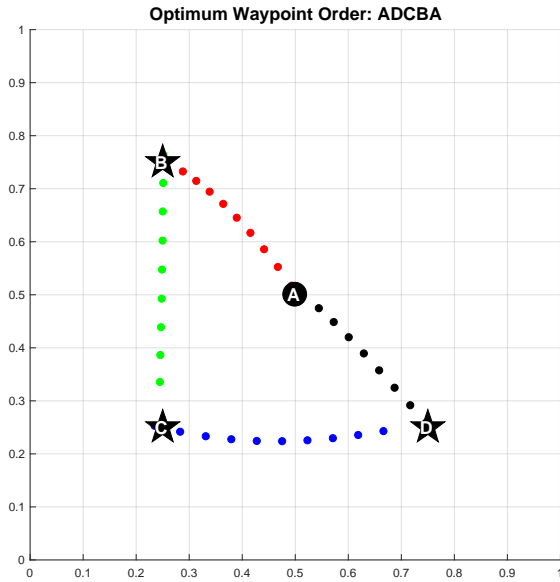
(b) Lower Frequency Current, $T_{current} = 1$
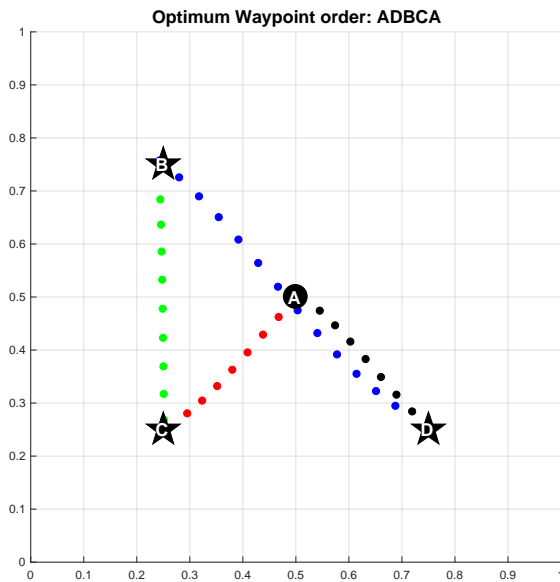
(c) Higher Frequency Current, $T_{current} = .5$

	Zero Current		Lower Frequency Current		Higher Frequency Current	
Path	Total Time *	% of Optimum **	Total Time *	% of Optimum **	Total Time *	% of Optimum **
ADCBA	**1.29**	**100%**	**1.15**	**100%**	1.35	111%
ADBCA	1.45	113%	1.49	130%	**1.22**	**100%**
ACDBA	1.45	113%	1.29	112%	1.45	119%
ACBDA	1.44	112%	1.51	131%	1.28	105%
ABDCA	1.44	112%	1.56	136%	1.49	122%
ABCDA	**1.29**	**100%**	1.37	119%	1.37	112%

* All times are unitless.

** Obtained by dividing tour duration by minimum duration for given scenario.

(d) Resulting Times

Figure 5-3: Test Case 2 demonstrates how varying a current temporally can produce dramatically different optimal paths for a given mission. Subfigure (c) shows a very non-intuitive optimal path which only results from an increase in current frequency. It is important to realize this non-intuitive mission path is actually faster than the original triangular path with no current.

5.1.3   Test Case 3: Parallel Front Visualization

Test Cases 1 and 2 have built intuition to show how this method works for a known, non-dimensional mission configuration. Test Case 3 makes the jump to real-world currents and locations with the goal to demonstrate how the reachability fronts are actually growing in parallel with each other. A vehicle begins at point A and is tasked to visit points B and C before returning to A. Points B and C are approximately 60 nautical miles and 40 nautical miles, respectively, from the starting point. The mission area is away from land to avoid complicating the plots, and local currents are between 0 and 1 knots of varying direction. The vehicle is traveling at 3 knots.

Figure 5-4 shows six snapshots in time during this two-waypoint mission. Subfigures 1 and 2 show how the initial reachability front grew from point A to points B and C. The front reaches point C first, as shown in the first subfigure. At this point in time, it is possible to plot the time-optimal path between points A and C. The time-optimal path from A to C is plotted in blue with the current along the path represented by the arrows. The color of the path itself corresponds to the vehicle's effective velocity while the color of the arrows corresponds to local current velocity.

Subfigure 2 shows the original black front continuing to grow while the new green front begins growing from point C. This plot captures the moment the original front reaches point B. The subfigures continue through time with the path ACBA shown in green and ABCA shown in red. Each plot captures a moment in time where one of the waypoints is reached and a time-optimal path can be shown. Subfigure 5 shows the earliest point in time that the mission can complete along the ACBA path. Subfigure 6 shows the final time that path ABCA completes.
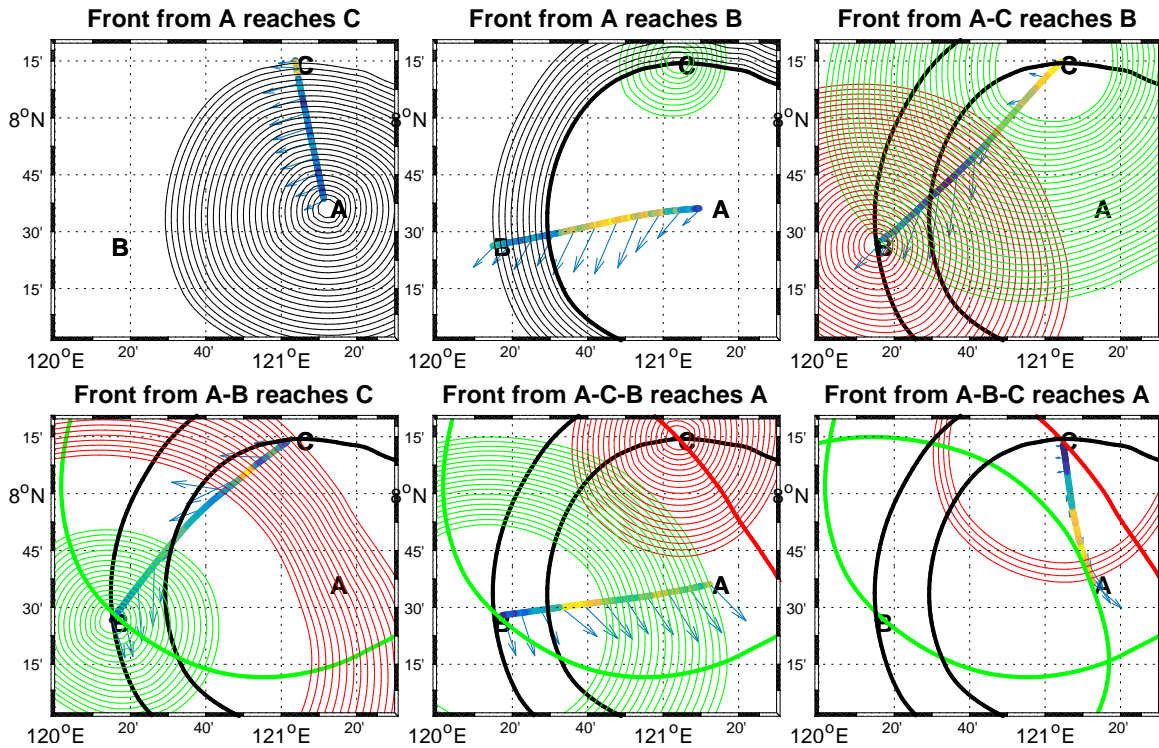
Figure 5-4: These six subfigures show how the five reachability front calculations progress through time. The reachability front from A to B & C is shown in black. The remaining calculations are shown in green for tour ACBA and red for tour ABCA. The time-optimal path is shown between points as the colored line where color describes the effective velocity. The current which influenced the path is shown by the arrows projecting from the path along the way.

5.2 Conceptual UUV Missions

The Philippines Archipelago region is an interesting operating area due to its complex geometry and strong dynamic currents. There are large-scale open ocean dynamics as well as small scale dynamics around islands, through narrow straits, and over steep shelfbreaks [Lermusiaux et al., 2011]. This area will be used to demonstrate several conceptual UUV missions. The first two missions will show two large three-waypoint missions of durations assumed within the range of the XLUUV (less than 30 days). Those will be followed by smaller five and six-waypoint missions within the LDUUV capability (less than 5 days).

5.2.1 Mission 1: Three-waypoint Shipwreck Inspection

Mission 1 demonstrates a vehicle leaving a central position and visiting the shipwreck sites of USS PC-1129 near Manila Bay, USS Barbel on the Southern tip of Palawan, and USS Cooper near the Port of Ormoc. By substituting "shipwrecks" with "subsea infrastructure", this could represent mission-type 5 of the RAND survey of UUV Mission, Monitoring Undersea Infrastructure (Section 1.2) [Button et al., 2009].

As the crow flies (a straight-line path ignoring currents and land), the targets are 166, 340, and 196 nautical miles from the starting location. Assuming a constant, 3 knots, the time-optimal tour, ABDCA, completes the mission in 18.83 days and the slowest tour, ADCBA, would take 24.6 hours or 5.4% longer.

The 5% improvement itself is not impressive, but there are several important points to consider about these results. A key takeaway is that the shortest-distance path is not necessarily the fastest. If the optimum order path is run in reverse (ACDBA), the mission would take 22.2 hours (4.9%) longer and is the second slowest time.

Figure 5-5 shows it is also important to consider that the overall geography may weigh into path selection. The second slowest path, ACBDA, takes a drastically different route, geographically, avoiding the narrow, complex route between D and C. It may be worth the additional 3.6 hours to avoid this area completely. Additionally, if there is a desire to avoid the long Northern (B-C) or North-Western (B-D) paths for operational reasons, this method would reveal the trade-offs in time associated with avoiding those areas.

It should also be pointed out that this mission plan assumes that the underlying current model is accurate. Realistically, lower confidence should be given to the model at times past its predictability limit, and missions this long are most likely beyond what a real-world current model can predict with high accuracy. A vehicle will most

likely need to receive updates throughout a mission this long in order to keep on a true optimal path. Finally, a 5% difference between best and worse-case paths means that other factors should be weighed more heavily than just waypoint-order when planning this mission. However, once the waypoint order is decided, there is no reason that these time-optimal paths should not be used.

In summary, Mission 1 shows some unique aspects of time-optimal mission planning but also gives perspective to some weaknesses inherent to the process. The latter can be addressed by existing MSEAS schema for uncertain currents (Subramani and Lermusiaux [2018]) and onboard routing (Lermusiaux et al. [2016]).

Path	Tour Duration (Days)	Hours beyond optimum	% of Optimum*
ADCBA	19.85	24.60	105.4%
ADBCA	19.58	18.00	104.0%
ACDBA	19.75	22.20	104.9%
ACBDA	18.97	3.50	100.8%
ABDCA	**18.83**	**0.00**	**100.0%**
ABCDA	19.40	13.70	103.0%

* Value obtained by dividing tour duration by the minimum tour duration

Figure 5-5: Mission 1 Results: First, all paths of all tour are shown with color corresponding to the list of tours and associated durations compared to the optimal. The optimum route, ABDCA, is then plotted separately with the color along the path (and color bar) corresponding to the vehicle's effective velocity. The arrows along the path show the magnitude and direction of the current along the way.

5.2.2 Mission 2: Three-Waypoint Constrained-Route Shipwreck Inspection

Mission 2 demonstrates a vehicle leaving the port of Ormoc and visiting the shipwreck sites of USS Ommaney Bay lying West of Panay Island, USS Samuel B. Roberts lying East of the Semirara Islands, and USS Princeton lying east of Lamon Bay. As the crow flies (a straight-line path ignoring currents and land), the targets are 200, 110, and 285 nautical miles from the starting location. Assuming a constant, 3 knots, the time-optimal path, ABCDA, completes the mission in 15.80 days and the slowest path, ACBDA, would take 2.35 days (15%) longer.

Figure 5-6 shows that the complex geography of the islands forced tight constraints on the vehicle paths, but nowhere is the time-optimal path a straight line. This demonstrates that the TOPP method is very useful, even in areas with little current. A human plotting these courses manually through complex island chains would be forced to string together hundreds of separate straight line segments into a vehicle path. The area where current can be seen to play the biggest role is the divergence of paths from C to D in the Western area. It is also interesting to notice that, depending on the time which the vehicle would pass the small crescent island in the South-Western area (Homonhon Island) the vehicle either went to the East or West of the island.

Given that this mission is only three waypoints, it is feasible that a human could have manually plotted courses for the all tour possibilities and narrowed down to either ABCDA or ADCBA as the two best choices (shortest distance). The difference of 12 hours can be considered negligible, given the uncertainties involved with 18-day time scale of the current model. However, as the number of waypoints scales a manual process becomes infeasible. To investigate this, missions with more waypoints will be explored.

All paths shown

Path	Tour Duration (Days)	Hours beyond optimum	% of Optimum*
ADCBA	16.31	12.10	103.2%
ADBCA	18.82	72.40	119.1%
ACDBA	16.80	23.80	106.3%
ACBDA	18.16	56.50	114.9%
ABDCA	17.16	32.50	108.6%
ABCDA	**15.80**	0.00	**100.0%**

* Value obtained by dividing tour duration by the minimum tour duration
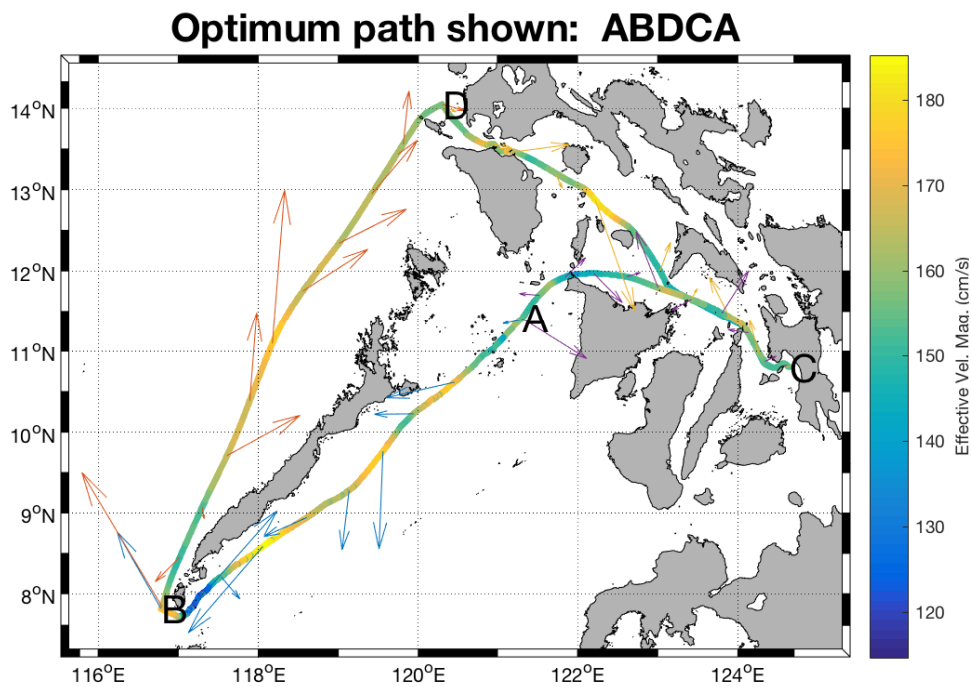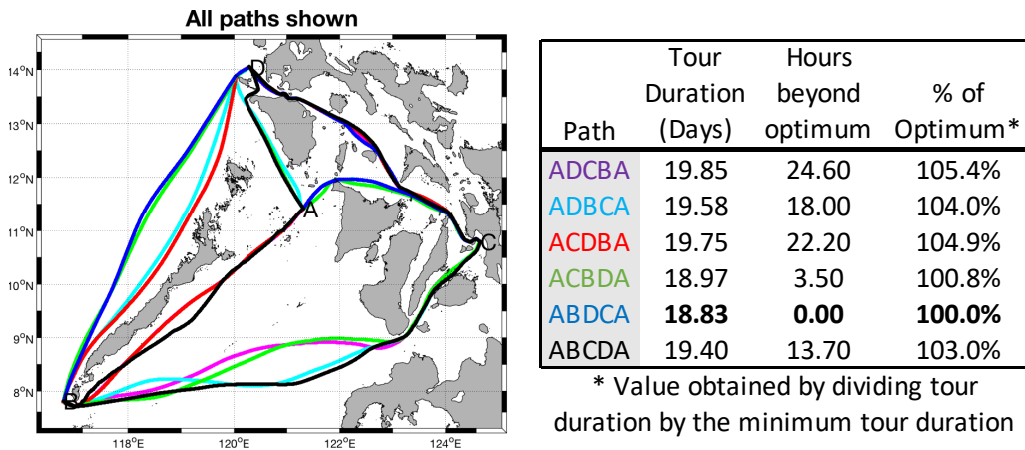
Optimum path shown: ABCDA

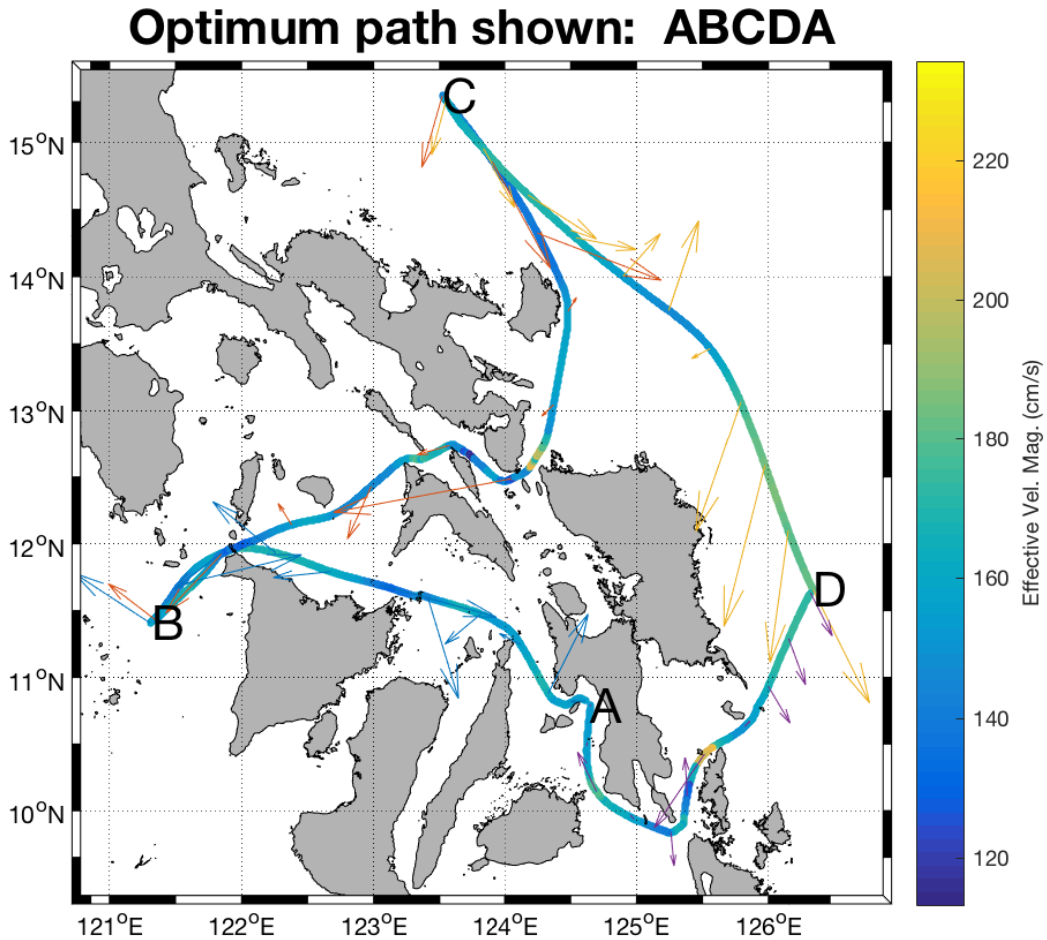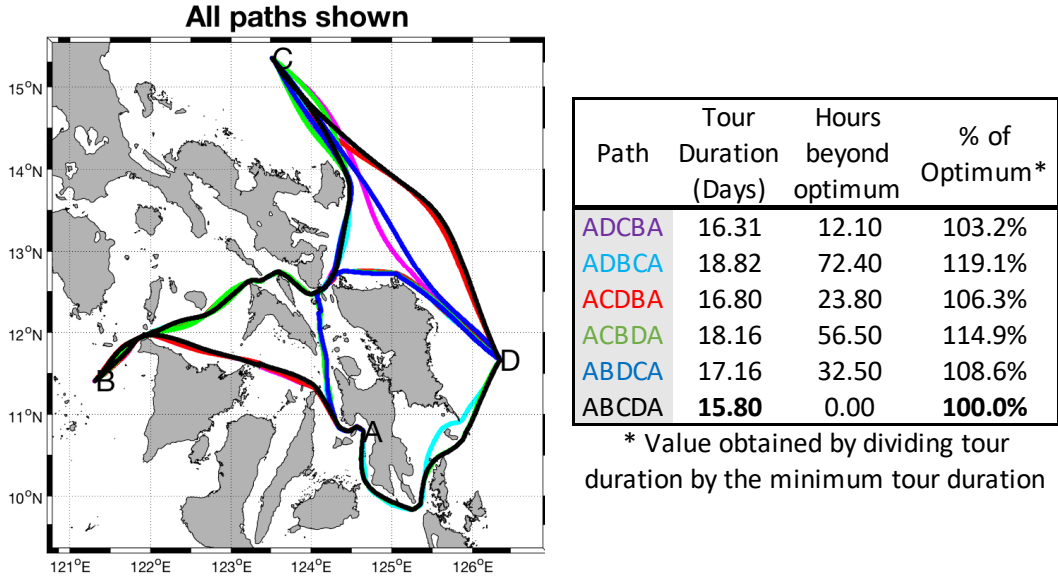Figure 5-6: Mission 2 Results: First, all paths of all tour are shown with color corresponding to the list of tours and associated durations compared to the optimal. The optimum route, ABCDA, is then plotted separately with the color along the path (and color bar) corresponding to the vehicle's effective velocity. The arrows along the path show the magnitude and direction of the current along the way.

31

5.2.3 Mission 3: Five-Waypoint Harbor Inspection Mission with Varying Start Times

For higher waypoint missions, there were multiple reasons to focus on smaller scale, LDUUV-type missions. As the number of waypoints increases, the number of reachability front calculations increases quickly. Additionally, as the distance between waypoints increases, the time per calculation increases. However, the most dramatic improvement comes from the fact that if the distances are smaller, a smaller current dataset can be used. For the TOPP solver implemented, the entire current grid is updated at every time step for U and V current velocities, and thus the computation time can be drastically improved by extracting a smaller data set. This does affect our results, as there is not point in using current data where it is known the UUV will not go (i.e. outside range of vehicle or inaccessible due to geography).

For the next example, an area around the Sulu Archipelago region was extracted as shown in Figure 5-7. This scenario represents mission-type 3 of the RAND survey of UUV missions, near-land and harbor monitoring (Section 1.2) [Button et al., 2009]. A UUV is launched from a surface ship (marked with a circle) and inspects five locations within a harbor (marked with stars). The inspection points were laid out in a perfect square with one point in the center, so that there were multiple tours with an identical straight-line distance. By varying the mission start times over the course of a few days, the same mission requires varying optimal paths as shown in Figure 5-8.

A five-waypoint mission produces 120 tours, requiring 326 reachability front calculations. The total computation time on the cluster for each mission plan was approximately 11 minutes. This highlights that smaller missions can be planned in real-time with the most recent current model available before launching a vehicle. This is feasible, and MSEAS has demonstrated the ability to re-compute real-time paths for real UUVs due to a change in operations [Subramani et al., 2017b].

Figure 5-7: Sulu Archipelago Five-Waypoint Mission Conditions: A smaller dataset, shown in red, was extracted from the larger dataset, shown in blue. This improves computational speed by removing areas the vehicle will never need to reach. The five objective locations were placed in a perfect square with one point in the middle. The mission was intended to simulate a UUV launched from a host ship and inspecting a harbor.
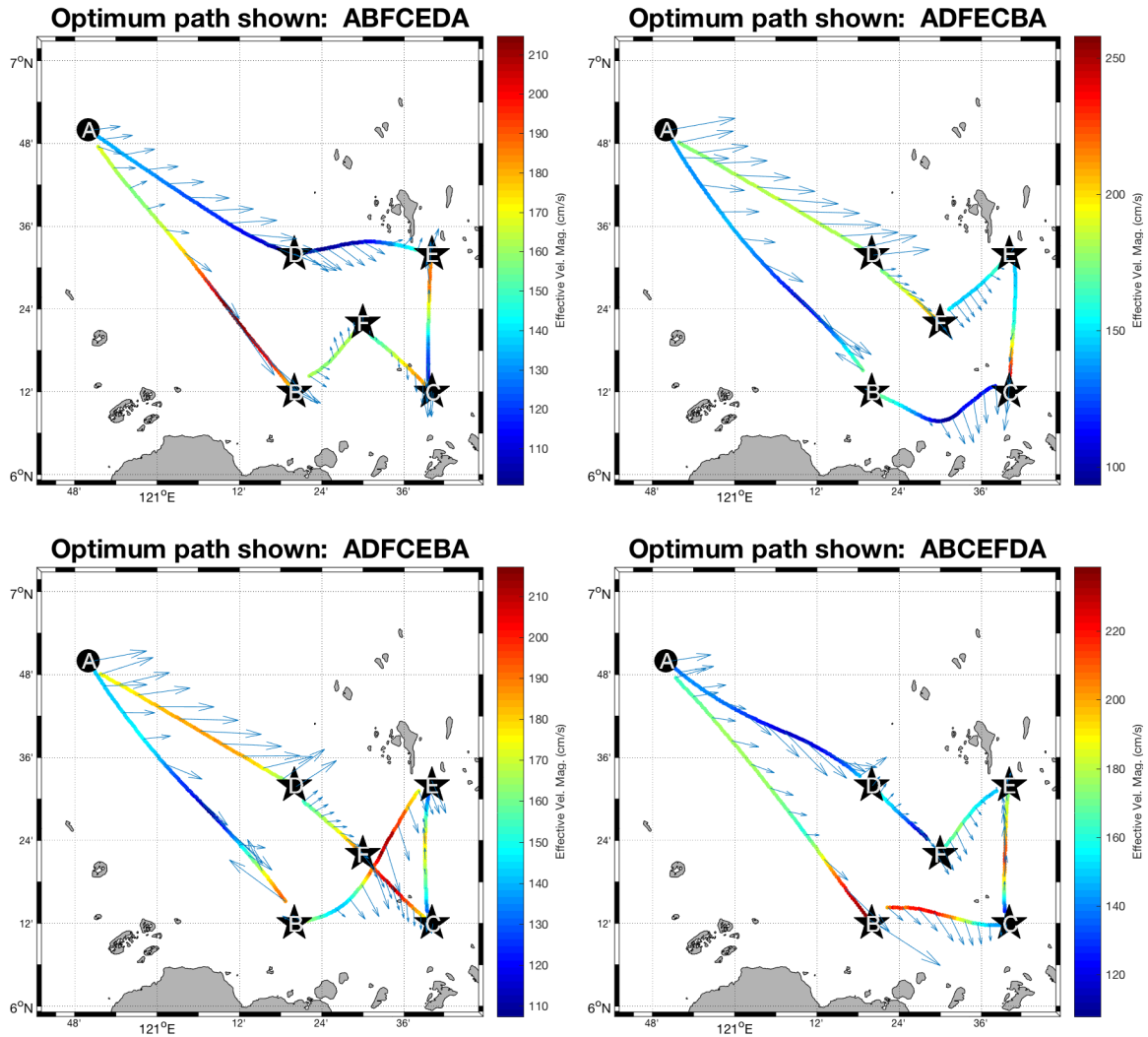
Figure 5-8: Mission 3: Harbor Inspection - The four paths shown are the optimal paths for the same mission with no change in mission setup except varying the time the vehicle was launched from the host ship. The color bar and color of the path show the vehicle's effective velocity, and the arrows show the speed and direction of the current along the way.

5.2.4 Mission 4: Six-waypoint Mine Clearance Mission

The traditional search for mines consists of driving "lawn-mower" patterns, scanning the bottom with active sonar, which is uniquely well accomplished by UUVs as recommended by the RAND survey. There is little for time-optimal path planning to contribute to this lawn-mower process since maintaining straight-line paths supports data collection. However, after processing of the sonar data, and identifying a number of mine-like objects, a follow up mission is normally required for closer inspection and/or neutralization at each location of interest. The next example illustrates a UUV traveling to six randomly placed objects near the Balabac Straight. Figure 5-9 shows both the area of data extracted and the mission initial conditions. The UUV starts its mission from a surface ship approximately 50 nm from the centroid of these objects. All six waypoints were randomly placed within a 40nm by 40 nm square and lie at a depth of approximately 100m of water.
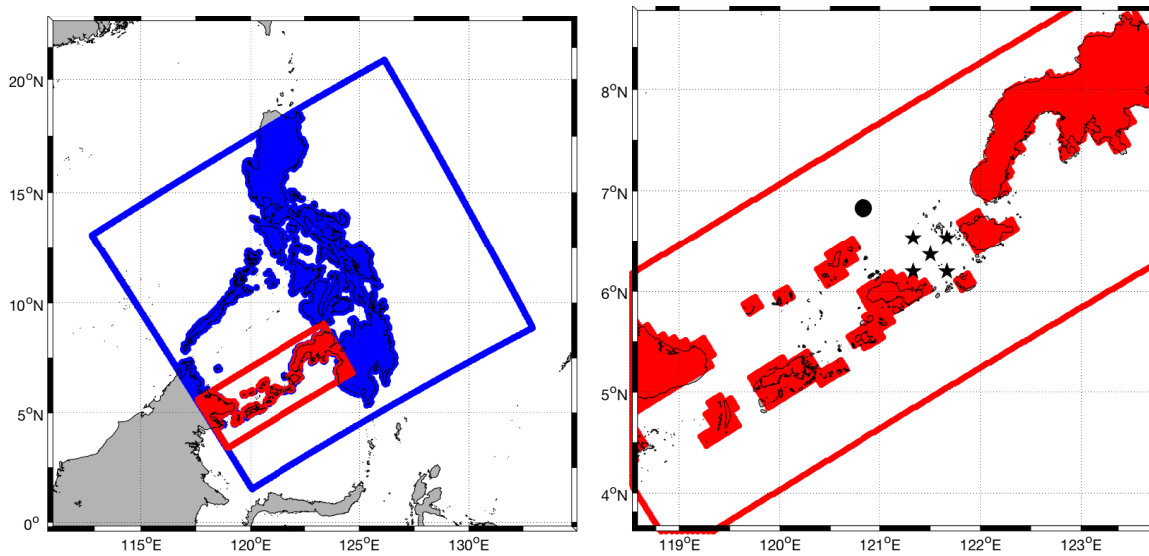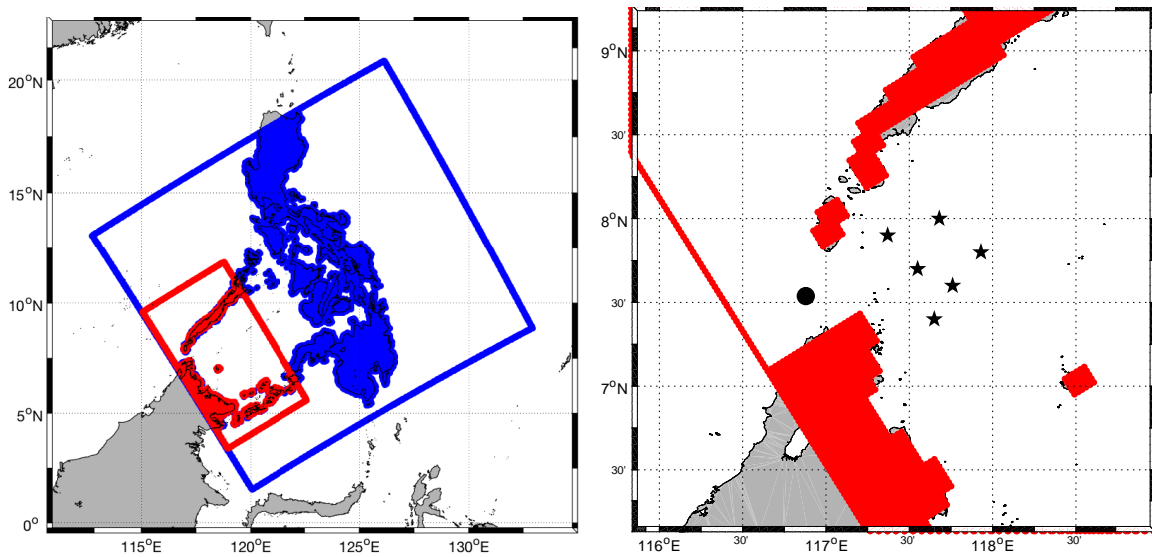

Figure 5-9: Balabac Straight Six-Waypoint Mission Conditions: A smaller dataset, shown in red, was extracted from the original dataset, shown in blue in order. This improves computational speed by removing areas the vehicle will never need to reach. The mission was intended to represent a mine clearance mission in which a vehicle is launched from a host ship in the straights and visits six randomly placed objectives.

All permutations of a six-waypoint mission result in 720 unique tours. The total durations of these tours are plotted in Figure 5-9. As is expected with many-city traveling salesman problems, there are a few tours which are close to being optimum and a wide range of tour which are nowhere near optimum. The fastest tour duration is 2.26 days while the slowest is 33 hours (61%) longer. The fastest four tours are

highlighted with red stars. The time-optimal paths of these four tours are shown in Figure 5-11.
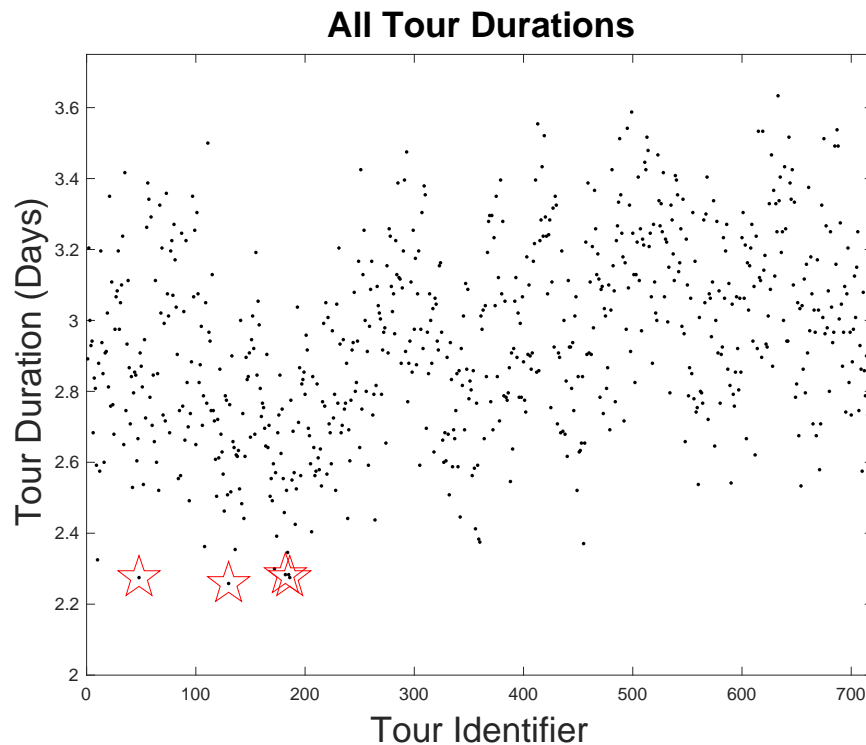
All Tour Durations

Figure 5-10: A six waypoint mission produces 720 permutations and their resulting tour durations. The four fastest tours are starred in red.

All four of these tours result in nominally the same duration, especially considering the inherent uncertainty of the current model. Therefore, this would present an operator with four tours to choose from. The best tour may be that which investigates a more important area first; the first subplots shows that tour AFGDCBEA would clear the northern shipping route first while the others would leave point G until later in the mission. The best tour may also avoid an enemy sensor or ship; the second subplot shows that tour AGEBCDFA would stay furthest from the island to the South-East.

The actual computation of all 720 tour durations resulted from the parallel processing of 1957 reachability front calculations, and the total processing time was 1 hour and 7 minutes. This computation time is much smaller than the actual mission durations of 2-3 days. Referring to Chapter 4, an infinite cluster could have processed up to 720 jobs in parallel. The MSEAS cluster has 440 nodes, and could have had other processes using resources at the time. Therefore, it is unlikely that more than 440 jobs could have been actually processing in parallel. This highlights how efficient

the process currently is and that there is room to improve processing speeds if needed for larger real-world mission.
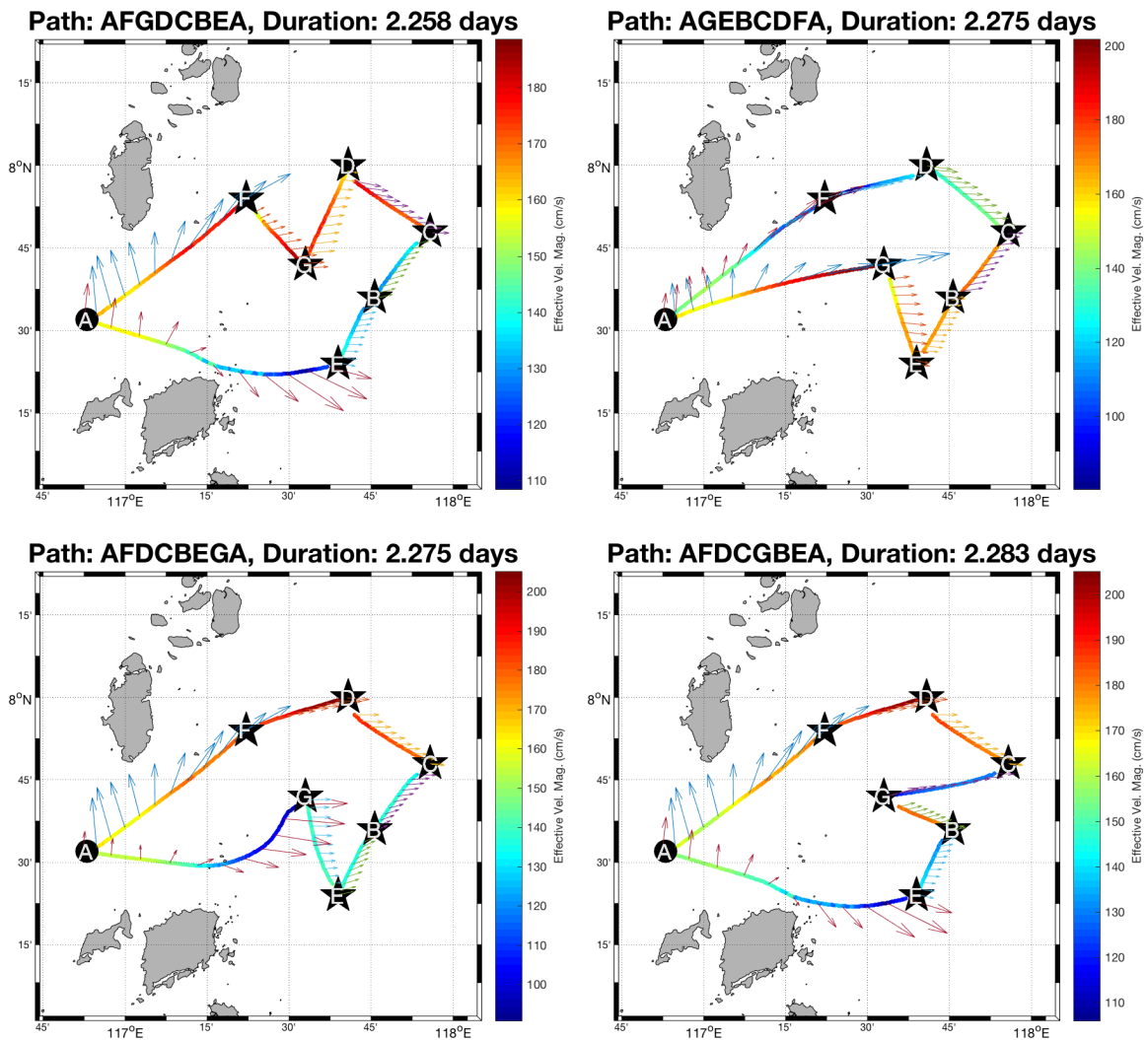
Figure 5-11: Mission 4: The four fastest tours of a mine clearance mission are shown. The durations are nearly equal, so they would present an operator or an autonomy software with four choices to complete a mission in a time-optimal fashion. The color bar and color of the path show the vehicle's effective velocity, and the arrows show the speed and direction of the current along the way.

Chapter 6

Conclusions and Future Work

6.1 Conclusions

This thesis has demonstrated the use of exact equations to predict time-optimal mission plans for a marine vehicle that visits a number of locations in a given dynamic ocean current field. By computing every permutation of this traveling salesman problem in dynamic currents, all variations in spatial and temporal dynamics are accounted for, ensuring the global optimum is known. Even though the method is very efficient and the optimal path can be computed serially in real-time for common naval operations, for additional computational speed, a high-performance computing cluster was used to solve the level set calculations in parallel. How these jobs were separated and executed in parallel was explained in detail with practical limitations addressed. It has been shown that mission plans can be calculated much faster than actual mission durations, and can therefore me used to update missions in real time. Future autonomous vehicles could either receive updates from the shore or calculate optimal tours and paths throughout a mission based on changing current forecasts or mission objectives.

This methodology was first applied to several hypothetical test cases to demonstrate different aspects of the theory. It was then validated for naval applications using an operational multi-resolution ocean modeling system of real-world current fields for the complex Philippines Archipelago region. Four conceptual UUV missions were shown which range in scale from small scale LDUUV missions lasting two days, to large scale XLUUV missions over two weeks long. All of these missions were computed efficiently and quickly enough to be used in real-time for actual missions.

Because the method calculates the global optimum, it serves two purposes. It can be used in its present form to plan multi-waypoint missions in conjunction with a predictive ocean current modeling system, or it can be used as a litmus test for

approximate future solutions to the traveling salesman problem in dynamic flow fields.

6.2 Future Work

As discussed in Chapter 2, there are countless other ways to optimize a marine vehicle's mission besides time. Future work could extend this method in order to account for other mission factors.

6.2.1 TSP Improvements

The goal of most TSP research has been to improve the computation speed by intelligently determining an optimal path without requiring all permutations to be calculated. Many basic TSP improvements such as path pruning could be applied to this thesis work to improve on the brute force method currently used. The size of the dataset could also be optimally chosen based on a give mission, but these improvements were outside the scope of this thesis. If a high-waypoint mission is to be planned on a large grid, especially with onboard electronics on a vehicle, then this method could become inefficient fairly quickly. However, by guaranteeing the global optimum is known, this method can be used as a litmus test for further research into this computationally difficult problem.

6.2.2 3D TOPP Integration

Currently, the model used assumes a constant depth for the vehicle. By integrating a 3D TOPP algorithm and 3D flow fields, there could be many interesting and useful results. For example, the vehicle could take advantage of vertical velocities as well as beneficial currents at various depths. In his Master's Thesis, Chinmay Kulkarni, developed a 3D TOPP and demonstrated its use in realistic currents with multiple vehicle types from UUVs to buoyancy gliders [Kulkarni, 2017].

6.2.3 Energy Optimization

Energy is the most common limiting factor for marine vehicles which are typically powered by an onboard battery. Extending this method to accounting for energy-optimal mission plans given the same current information is the first step down this path. However, by incorporating other data into the model, there could be further improvements. For example, a cloud cover model could be combined so that a solar powered surface vehicle is simultaneously expending power to move and taking in

power from the sun. Additionally, a sea state model could be incorporated to provide speed inputs for a wave glider [Kulkarni, 2017].

6.2.4   Orienteering Problem

In the classic orienteering problem, the goal is determine what subset of a large set of waypoints can be visited and in what order, given a time limit. Weights could be assigned to each waypoint, communicated its relative importance, and the goal of the solver would be to maximize a mission's score within its energy and/or time requirements [Gunawan et al., 2016].

6.2.5   Moving Tasks and Masks

To further add complications and realism to the problem, the waypoints themselves could be allowed to move. This could represent a mission which must observe moving targets along with visiting stationary waypoints. Additionally, stay out zones around moving objects could be represented by a moving mask within the current model [Lolla et al., 2015; Mirabito et al., 2017].

6.2.6   Real World Testing

While a real-world test of the TOPP algorithm has been demonstrated between two points, to fully demonstrate this capability in a real UUV mission, there are several steps remaining. A predictive current model must be generated for the operating area in the days or hours leading up to the vehicle launch. The results of this method can then be used as inputs to the vehicle's onboard navigation software. The vehicle would need to "race" an identical vehicle at the same time in order to compare results.

Bibliography

Agarwal, A. (2009). *Statistical Field Estimation and Scale Estimation for Complex Coastal Regions and Archipelagos*. Master's thesis, Massachusetts Institute of Technology, Department of Mechanical Engineering, Cambridge, Massachusetts.

Agarwal, A. and Lermusiaux, P. F. J. (2011). Statistical field estimation for complex coastal regions and archipelagos. *Ocean Modelling*, 40(2):164–189.

Applegate, D. L. (2006). *The traveling salesman problem : a computational study*. Princeton series in applied mathematics. Princeton : Princeton University Press, c2006.

Beşiktepe, Ş. T., Lermusiaux, P. F. J., and Robinson, A. R. (2003). Coupled physical and biogeochemical data-driven simulations of Massachusetts Bay in late summer: real-time and post-cruise data assimilation. *Journal of Marine Systems*, 40–41:171–212.

Burton, L. J. (2009). *Modeling Coupled Physics and Biology in Ocean Straits with Application to the San Bernardino Strait in the Philippine Archipelago*. Master's thesis, Massachusetts Institute of Technology, Department of Mechanical Engineering, Cambridge, Massachusetts.

Button, R. W., Kamp, J., Curtin, T. B., and Dryden, J. (2009). A Survey of Missions for Unmanned Undersea Vehicles.

Carolis, V. D. (2017). Runtime Energy Estimation and Route Optimization for Autonomous Underwater Vehicles. *IEEE Journal of Oceanic Engineering, Oceanic Engineering, IEEE Journal of, IEEE J. Oceanic Eng.*, (99):1.

Carolis, V. D., Lane, D. M., and Brown, K. E. (2014). Low-cost energy measurement and estimation for autonomous underwater vehicles. In *OCEANS 2014 - TAIPEI*, pages 1–5.

Chien-Chou, S., Yih, Y., Mong-Fong, H., Tien-Szu, P., and Jeng-Shyang, P. (2014). A framework to evolutionary path planning for autonomous underwater glider. In *Modern Advances in Applied Intelligence*, Lecture Notes in Computer Science, pages 1–11. Springer, Cham.

Colin, M. E. G. D., Duda, T. F., te Raa, L. A., van Zon, T., Haley, Jr., P. J., Lermusiaux, P. F. J., Leslie, W. G., Mirabito, C., Lam, F. P. A., Newhall, A. E., Lin, Y.-T., and Lynch, J. F. (2013). Time-evolving acoustic propagation modeling in a complex ocean environment. In *OCEANS - Bergen, 2013 MTS/IEEE*, pages 1–9.

Cossarini, G., Lermusiaux, P. F. J., and Solidoro, C. (2009). Lagoon of Venice ecosystem: Seasonal dynamics and environmental guidance with uncertainty analyses and error subspace data assimilation. *Journal of Geophysical Research: Oceans*, 114(C6).

Duda, T. F., Lin, Y.-T., Zhang, W., Cornuelle, B. D., and Lermusiaux, P. F. J. (2011). Computational studies of three-dimensional ocean sound fields in areas of complex seafloor topography and active ocean dynamics. In *Proceedings of the 10th International Conference on Theoretical and Computational Acoustics*, Taipei, Taiwan.

Edwards, J., Smith, J., Girard, A., Wickman, D., Subramani, D. N., Kulkarni, C. S., Haley, Jr., P. J., Mirabito, C., Jana, S., and Lermusiaux, P. F. J. (2017). Data-driven learning and modeling of AUV operational characteristics for optimal path planning. In *Oceans '17 MTS/IEEE Conference*, Aberdeen.

Evangelinos, C., Lermusiaux, P. F. J., Geiger, S. K., Chang, R. C., and Patrikalakis, N. M. (2006). Web-enabled configuration and control of legacy codes: An application to ocean modeling. *Ocean Modelling*, 13(3):197–220.

Evangelinos, C., Lermusiaux, P. F. J., Xu, J., Haley, P. J., and Hill, C. N. (2011). Many task computing for real-time uncertainty prediction and data assimilation in the ocean. *IEEE Transactions on Parallel and Distributed Systems*, 22(6):1012–1024. Special Section on Many-Task Computing.

Gangopadhyay, A., Lermusiaux, P. F., Rosenfeld, L., Robinson, A. R., Calado, L., Kim, H. S., Leslie, W. G., and Haley, Jr., P. J. (2011). The California Current system: A multiscale overview and the development of a feature-oriented regional modeling system (FORMS). *Dynamics of Atmospheres and Oceans*, 52(1–2):131–169. Special issue of Dynamics of Atmospheres and Oceans in honor of Prof. A. R. Robinson.

Gawarkiewicz, G., Jan, S., Lermusiaux, P. F. J., McClean, J. L., Centurioni, L., Taylor, K., Cornuelle, B., Duda, T. F., Wang, J., Yang, Y. J., Sanford, T., Lien, R.-C., Lee, C., Lee, M.-A., Leslie, W., Haley, Jr., P. J., Niiler, P. P., Gopalakrishnan, G., Velez-Belchi, P., Lee, D.-K., and Kim, Y. Y. (2011). Circulation and intrusions northeast of Taiwan: Chasing and predicting uncertainty in the cold dome. *Oceanography*, 24(4):110–121.

Gerlack, J. (2015). Autonomous data collection techniques for approximating marine vehicle kinematics. Master's thesis, Massachusetts Institute of Technology, Department of Mechanical Engineering, Cambridge, Massachusetts.

Gunawan, A., Lau, H. C., and Vansteenwegen, P. (2016). Orienteering Problem: A survey of recent variants, solution approaches and applications. *European Journal of Operational Research*, 255(2):315–332.

Haley, Jr., P. J., Agarwal, A., and Lermusiaux, P. F. J. (2015). Optimizing velocities and transports for complex coastal regions and archipelagos. *Ocean Modeling*, 89:1–28.

Haley, Jr., P. J. and Lermusiaux, P. F. J. (2010). Multiscale two-way embedding schemes for free-surface primitive equations in the "Multidisciplinary Simulation, Estimation and Assimilation System". *Ocean Dynamics*, 60(6):1497–1537.

Haley, Jr., P. J., Lermusiaux, P. F. J., Robinson, A. R., Leslie, W. G., Logoutov, O., Cossarini, G., Liang, X. S., Moreno, P., Ramp, S. R., Doyle, J. D., Bellingham, J., Chavez, F., and Johnston, S. (2009). Forecasting and reanalysis in the Monterey Bay/California Current region for the Autonomous Ocean Sampling Network-II experiment. *Deep Sea Research Part II: Topical Studies in Oceanography*, 56(3–5):127–148.

Kulkarni, C. S. (2017). Three-dimensional time-optimal path planning in dynamic and realistic environments. Master's thesis, Massachusetts Institute of Technology, Department of Mechanical Engineering, Cambridge, Massachusetts.

Lam, F. (2005). *Traveling salesman path problems*. Thesis, Massachusetts Institute of Technology, Cambridge, Massachusetts.

Lam, F.-P. A., Haley, Jr., P. J., Janmaat, J., Lermusiaux, P. F. J., Leslie, W. G., Schouten, M. W., te Raa, L. A., and Rixen, M. (2009). At-sea real-time coupled four-dimensional oceanographic and acoustic forecasts during Battlespace Preparation 2007. *Journal of Marine Systems*, 78(Supplement):S306–S320.

Leavitt, J. W. (2017). Intent-aware collision avoidance for autonomous marine vehicles. Master's thesis, Massachusetts Institute of Technology, Department of Mechanical Engineering, Cambridge, Massachusetts.

Lermusiaux, P. F. J. (2002). On the mapping of multivariate geophysical fields: Sensitivities to size, scales, and dynamics. *Journal of Atmospheric and Oceanic Technology*, 19(10):1602–1637.

Lermusiaux, P. F. J. (2006). Uncertainty estimation and prediction for interdisciplinary ocean dynamics. *Journal of Computational Physics*, 217(1):176–199.

Lermusiaux, P. F. J. (2007). Adaptive modeling, adaptive data assimilation and adaptive sampling. *Physica D: Nonlinear Phenomena*, 230(1):172–196.

Lermusiaux, P. F. J., Anderson, D. G. M., and Lozano, C. J. (2000). On the mapping of multivariate geophysical fields: Error and variability subspace estimates. *Quarterly Journal of the Royal Meteorological Society*, 126(565):1387–1429.

Lermusiaux, P. F. J., Chiu, C.-S., Gawarkiewicz, G. G., Abbot, P., Robinson, A. R., Miller, R. N., Haley, Jr, P. J., Leslie, W. G., Majumdar, S. J., Pang, A., and Lekien, F. (2006). Quantifying uncertainties in ocean predictions. *Oceanography*, 19(1):92–105.

Lermusiaux, P. F. J., Haley, P. J., Leslie, W. G., Agarwal, A., Logutov, O., and Burton, L. J. (2011). Multiscale physical and biological dynamics in the Philippine Archipelago: Predictions and processes. *Oceanography*, 24(1):70–89. Special Issue on the Philippine Straits Dynamics Experiment.

Lermusiaux, P. F. J., Haley, Jr., P. J., Gawarkiewicz, G. G., and Jan, S. (2018). Evaluation of multiscale ocean probabilistic forecasts: Quantifying, predicting and exploiting uncertainty. In preparation.

Lermusiaux, P. F. J., Haley, Jr., P. J., Jana, S., Gupta, A., Kulkarni, C. S., Mirabito, C., Ali, W. H., Subramani, D. N., Dutt, A., Lin, J., Shcherbina, A., Lee, C., and Gangopadhyay, A. (2017a). Optimal planning and sampling predictions for autonomous and lagrangian platforms and sensors in the northern Arabian Sea. *Oceanography*, 30(2):172–185. Special issue on Autonomous and Lagrangian Platforms and Sensors (ALPS).

Lermusiaux, P. F. J., Haley, Jr, P. J., and Yilmaz, N. K. (2007). Environmental prediction, path planning and adaptive sampling: sensing and modeling for efficient ocean monitoring, management and pollution control. *Sea Technology*, 48(9):35–38.

Lermusiaux, P. F. J., Lolla, T., Haley, Jr., P. J., Yigit, K., Ueckermann, M. P., Sondergaard, T., and Leslie, W. G. (2016). Science of autonomy: Time-optimal path planning and adaptive sampling for swarms of ocean vehicles. In Curtin, T., editor, *Springer Handbook of Ocean Engineering: Autonomous Ocean Vehicles, Subsystems and Control*, chapter 21, pages 481–498. Springer.

Lermusiaux, P. F. J., Malanotte-Rizzoli, P., Stammer, D., Carton, J., Cummings, J., and Moore, A. M. (2006). Progress and prospects of U.S. data assimilation in ocean research. *Oceanography*, 19(1):172–183.

Lermusiaux, P. F. J., Subramani, D. N., Lin, J., Kulkarni, C. S., Gupta, A., Dutt, A., Lolla, T., Haley, Jr., P. J., Ali, W. H., Mirabito, C., and Jana, S. (2017b). A future for intelligent autonomous ocean observing systems. *Journal of Marine Research*, 75. Special issue: The Science of Ocean Prediction, vol. 17 of The Sea. In press.

Lermusiaux, P. F. J., Xu, J., Chen, C.-F., Jan, S., Chiu, L., and Yang, Y.-J. (2010). Coupled ocean–acoustic prediction of transmission loss in a continental shelfbreak region: Predictive skill, uncertainty quantification, and dynamical sensitivities. *IEEE Journal of Oceanic Engineering*, 35(4):895–916.

Leslie, W. G., Robinson, A. R., Haley, Jr, P. J., Logutov, O., Moreno, P. A., Lermusiaux, P. F. J., and Coelho, E. (2008). Verification and training of real-time

forecasting of multi-scale ocean dynamics for maritime rapid environmental assessment. *Journal of Marine Systems*, 69(1):3–16.

Liao, Y., Wang, L., Li, Y., Li, Y., and Jiang, Q. (2016). The intelligent control system and experiments for an unmanned wave glider. 11(12):e0168792–e0168792.

Logutov, O. G. and Lermusiaux, P. F. J. (2008). Inverse barotropic tidal estimation for regional ocean applications. *Ocean Modelling*, 25(1–2):17–34.

Lolla, T., Haley, Jr., P. J., and Lermusiaux, P. F. J. (2014a). Time-optimal path planning in dynamic flows using level set equations: Realistic applications. *Ocean Dynamics*, 64(10):1399–1417.

Lolla, T., Haley, Jr., P. J., and Lermusiaux, P. F. J. (2015). Path planning in multi-scale ocean flows: coordination and dynamic obstacles. *Ocean Modelling*, 94:46–66.

Lolla, T., Lermusiaux, P. F. J., Ueckermann, M. P., and Haley, Jr., P. J. (2014b). Time-optimal path planning in dynamic flows using level set equations: Theory and schemes. *Ocean Dynamics*, 64(10):1373–1397.

Lolla, T., Ueckermann, M. P., Yiğit, K., Haley, Jr., P. J., and Lermusiaux, P. F. J. (2012). Path planning in time dependent flow fields using level set methods. In *IEEE International Conference on Robotics and Automation (ICRA), 14-18 May 2012*, pages 166–173.

Mirabito, C., Subramani, D. N., Lolla, T., Haley, Jr., P. J., Jain, A., Lermusiaux, P. F. J., Li, C., Yue, D. K. P., Liu, Y., Hover, F. S., Pulsone, N., Edwards, J., Railey, K. E., and Shaw, G. (2017). Autonomy for surface ship interception. In *Oceans '17 MTS/IEEE Conference*, Aberdeen.

Onken, R., Robinson, A. R., Lermusiaux, P. F. J., Haley, P. J., and Anderson, L. A. (2003). Data-driven simulations of synoptic circulation and transports in the Tunisia-Sardinia-Sicily region. *Journal of Geophysical Research: Oceans*, 108(C9).

Pan, Y., P. H. J. and Lermusiaux, P. (2018). Interaction of internal tide with a heterogeneous and rotational ocean background. *Journal of Fluid Mechanics*. Sub-judice.

Ramp, S. R., Davis, R. E., Leonard, N. E., Shulman, I., Chao, Y., Robinson, A. R., Marsden, J., Lermusiaux, P. F. J., Fratantoni, D. M., Paduan, J. D., Chavez, F. P., Bahr, F. L., Liang, S., Leslie, W., and Li, Z. (2009). Preparing to predict: The second Autonomous Ocean Sampling Network (AOSN-II) experiment in the Monterey Bay. *Deep Sea Research Part II: Topical Studies in Oceanography*, 56(3–5):68–86.

Ramp, S. R., Lermusiaux, P. F. J., Shulman, I., Chao, Y., Wolf, R. E., and Bahr, F. L. (2011). Oceanographic and atmospheric conditions on the continental shelf north of the Monterey Bay during August 2006. *Dynamics of Atmospheres and*

Oceans, 52(1–2):192–223. Special issue of Dynamics of Atmospheres and Oceans in honor of Prof. A. R. Robinson.

Schofield, O., Glenn, S., Orcutt, J., Arrott, M., Meisinger, M., Gangopadhyay, A., Brown, W., Signell, R., Moline, M., Chao, Y., Chien, S., Thompson, D., Balasuriya, A., Lermusiaux, P. F. J., and Oliver, M. (2010). Automated sensor networks to advance ocean science. *Eos Trans. AGU*, 91(39):345–346.

Subramani, D. N. (2018). *Probabilistic Regional Ocean Predictions: Stochastic Fields and Optimal Planning*. PhD thesis, Massachusetts Institute of Technology, Department of Mechanical Engineering, Cambridge, Massachusetts.

Subramani, D. N., Haley, Jr., P. J., and Lermusiaux, P. F. J. (2017a). Energy-optimal path planning in the coastal ocean. *Journal of Geophysical Research: Oceans*, 122:3981–4003.

Subramani, D. N. and Lermusiaux, P. F. J. (2016). Energy-optimal path planning by stochastic dynamically orthogonal level-set optimization. *Ocean Modeling*, 100:57–77.

Subramani, D. N. and Lermusiaux, P. F. J. (2018). Risk-optimal path planning in uncertain, strong and dynamic flows. In preparation.

Subramani, D. N., Lermusiaux, P. F. J., Haley, Jr., P. J., Mirabito, C., Jana, S., Kulkarni, C. S., Girard, A., Wickman, D., Edwards, J., and Smith, J. (2017b). Time-optimal path planning: Real-time sea exercises. In *Oceans '17 MTS/IEEE Conference*, Aberdeen.

Subramani, D. N., Wei, Q. J., and Lermusiaux, P. F. J. (2018). Stochastic time-optimal path-planning in uncertain, strong, and dynamic flows. *Computer Methods in Applied Mechanics and Engineering*, 333:218–237.

Ueckermann, M. P. (2014). *High Order Hybrid Discontinuous Galerkin Regional Ocean Modeling*. PhD thesis, Massachusetts Institute of Technology, Department of Mechanical Engineering, Cambridge, MA.

Ueckermann, M. P. and Lermusiaux, P. F. J. (2012). 2.29 Finite Volume MATLAB Framework Documentation. MSEAS Report 14, Department of Mechanical Engineering, Massachusetts Institute of Technology, Cambridge, MA.

Ueckermann, M. P. and Lermusiaux, P. F. J. (2016). Hybridizable discontinuous Galerkin projection methods for Navier–Stokes and Boussinesq equations. *Journal of Computational Physics*, 306:390–421.

Ueckermann, M. P., Mirabito, C., Haley, Jr., P. J., and Lermusiaux, P. F. J. (2018). High Order Hybridizable Discontinuous Galerkin Projection Schemes for Non-hydrostatic Physical-Biogeochemical Ocean Modeling. In preparation.

US Navy (2004). The navy unmanned undersea vehicle (UUV) master plan. OCLC: 832063493.

US Navy Undersea Warfare Directorate (2016). Autonomous undersea vehicle requirement for 2025. OCLC: 945667105.

Woerner, K. (2017). Multi-contact protocol-constrained collision avoidance for autonomous marine vehicles. Master's thesis, Massachusetts Institute of Technology, Department of Mechanical Engineering, Cambridge, Massachusetts.

Xu, J., Lermusiaux, P. F. J., Haley Jr., P. J., Leslie, W. G., and Logutov, O. G. (2008). Spatial and Temporal Variations in Acoustic propagation during the PLUSNet-07 Exercise in Dabob Bay. In *Proceedings of Meetings on Acoustics (POMA)*, volume 4, page 11. Acoustical Society of America 155th Meeting.

Ziezulewicz, G. (2017). Navy stands up first underwater drone squadron. *Navy Times*.